

Modeling the impact of climate change on the hydrology of  
Eagle Mountain Lake, Texas

by

Daniel Ayomikun Ayejoto

Bachelor of Science in Industrial Chemistry, 2017  
University of Ilorin, Nigeria

Submitted to the Graduate Faculty of  
the College of Science and  
Engineering Texas Christian  
University

in partial fulfillment of the  
requirements for the degree of

Master of Science

May 2024

Copyright by  
Daniel Ayomikun Ayejoto  
2024

## ACKNOWLEDGEMENTS

First and foremost, I offer my deepest gratitude to God for His boundless mercies, unwavering strength, and grace that sustained me throughout the journey of completing this work.

I extend my heartfelt appreciation to Dr. Gehendra Kharel, my advisor, whose invaluable guidance, unwavering support, and constant encouragement were instrumental in every stage of researching and writing this thesis. His expertise and insightful feedback have significantly shaped this work.

I am equally grateful to Dr. Brendran Lavy and Professor Michele Birmingham, esteemed members of my thesis committee, for their invaluable input, insightful comments, and constructive suggestions, which greatly enhanced the quality of this thesis.

To the faculty and staff of the Department of Environmental and Sustainability Sciences at Texas Christian University, I express my sincere appreciation for fostering an environment of academic excellence that provided the necessary resources and support conducive to meaningful learning and research endeavors.

To my beloved family—Mr. and Mrs. Ayejoto, and my dear siblings Stella Tolulope Ayejoto and Samuel Segun Ayejoto—I owe an immeasurable debt of gratitude. Your unwavering love, support, and understanding have been the bedrock of my academic pursuits, sustaining me through every challenge and triumph.

To each and every one of you who has played a part, big or small, in this remarkable journey, I offer my sincerest gratitude. Your presence and support have made all the difference, and for that, I am deeply grateful.

# Table of Contents

ACKNOWLEDGEMENTS.....	iii
LIST OF TABLES .....	vi
LIST OF FIGURES.....	viii
CHAPTER I .....	1
INTRODUCTION.....	1
Research Background .....	1
Water Resources and Climate Change in Texas.....	6
CHAPTER II.....	10
REVIEW OF LITERATURE.....	10
CHAPTER III.....	14
METHODOLOGY .....	14
Study Area .....	14
Hydrological Model (SWAT).....	17
Watershed Data for SWAT Model .....	19
Topographic Information.....	20
Land Use and Land Cover.....	21
Soil Data .....	21
Climate Data .....	23
Streamflow Data .....	24
SWAT Model Setup .....	27
Watershed Delineation .....	28
Hydrological Response Unit processing.....	29
Writing Input Data Table.....	32
SWAT Model Run.....	33
SWAT Model Calibration, Validation, and Sensitivity Analysis.....	34
Sub-basin 10 .....	37
Sub-basin 15 .....	39
Sub-basin 22 .....	41
Sub-basin 24 .....	42
Model Performance Analysis .....	44
Future Climate Scenarios.....	46

Introduction to LARS-WG .....	46
How LARS-WG Works.....	47
Site Analysis .....	47
Creating climate scenarios from GCM output.....	50
CHAPTER IV .....	57
RESULTS.....	57
Model Calibration and Validation .....	57
Sub-basin 10 .....	57
Sub-basin 15 .....	58
Sub-basin 22 .....	58
Sub-basin 24 .....	59
Historical Climate Data (1990-2022) .....	59
Future vs Historical Climate Data Analysis .....	64
Annual Streamflow .....	73
Monthly Streamflow .....	77
CHAPTER V.....	82
DISCUSSION .....	82
Model Performance .....	82
Impacts of Climate Change in the Study Watershed.....	84
Impacts of Climate Change on Streamflow.....	86
Model Limitations .....	91
Recommendation .....	93
CHAPTER VI .....	95
Conclusion.....	95
References .....	96

VITA

ABSTRACT

## LIST OF TABLES

Table 3.1. Input data and their sources for developing the hydrological model of the watershed .....	19
Table 3.2. Description of Hydrologic Soil Groups (HSG) (USDA, 2020).....	22
Table 3.3. Climate Stations used in the Upper West Fork Watershed Model .....	24
Table 3.4. Streamflow gauge stations used in the Upper West Fork Watershed model.....	25
Table 3.5. A list of model parameters and their sensitivities to streamflow in the study watershed .....	36
Table 3.6. Calibrated parameters for the West Fork Trinity River near Jacksboro, Texas (Sub-basin 10).....	38
Table 3.7. Calibrated parameters for the Big Sandy Creek near Bridgeport, Texas (Sub-basin 15).....	40
Table 3.8. Calibrated parameters for the West Fork Trinity River near Boyd, Texas (Sub-basin 22).....	41
Table 3.9. Calibrated parameters for the Walnut Creek at Reno, Texas (Sub-basin 24).....	43
Table 3.10. GCMs from CMIP6 integrated with LARS-WG.....	51
Table 3.11. Overview of CMIP6 scenarios and their corresponding SSPs .....	55
Table 4.1. Summary of Calibration and Validation Results for Streamflow Simulation in Different Sub-basins .....	57
Table 4.2. Comparative analysis of future temperature projections (2030s and 2080s) and historical temperature (1990-2022) for seven stations in the study watershed.....	65

Table 4.3. Comparative analysis of future precipitation projections (2030s and 2080s) and historical precipitation (1990-2022) for seven stations in the study watershed.....	70
Table 4.4. Average annual streamflow under different climate scenarios.....	75
Table 4.5. Average monthly streamflow under different climate scenarios in the study watershed .....	79
Table 4.6. Percentage (%) change in future monthly streamflow compared to the historical climate.....	79

## LIST OF FIGURES

Figure 3.1 The Upper West Fork Trinity Watershed with major land cover and streamflow stations .....	16
Figure 3.2 Eagle Mountain Lake located in Region C (black circle in the map), North Texas area (Source: TWDB, 2022b; Eagle-Mountain-guide, 2017).....	17
Figure 3.3. Elevation gradient in the study watershed.....	20
Figure 3.4. Flowchart illustrating the research methodology employed to assess the impacts of climate change on the study watershed hydrology using soil and water assessment tool (SWAT).....	28
Figure 3.5. Soil hydrologic groups in the study watershed.....	31
Figure 3.6. Slope Map.....	32
Figure 3.7. SWAT model simulation setup .....	34

# CHAPTER I

## INTRODUCTION

### Research Background

Climate change is a crucial issue with documented effects on natural and human systems today. Among many reported impacts, such as melting ice caps, ocean acidification, and biodiversity loss, climate change impacts on terrestrial hydrology, including water availability as measured in terms of droughts and floods, are of critical concern (Hoegh-Guldberg et al., 2019; Mariappan et al., 2023; Talukder et al., 2022). Over the last two decades (2001–2021), climate change, with changes in long-term precipitation and temperature, has produced noticeable impacts around the world, leading to pronounced alterations in the amount and levels of surface water and groundwater (Abbass et al., 2022; CBF, 2020). The Intergovernmental Panel on Climate Change (IPCC) Fifth Assessment Report stated that for every degree Celsius increase in global average temperature, the global mean precipitation events are projected to increase by about 7% (IPCC, 2014a). With global temperatures projected to increase by 1.8 to 2.8°C by the end of the 21st century, compared to 0.8°C change in the 20th century, global precipitation intensity could increase by 12.6% to 19.6% in the coming decades (Noor et al., 2022). As a result of the projected changes in precipitation and temperature, there will be significant impacts on the hydrological cycle, leading to an increased frequency and intensity of droughts and floods. These events will have far-reaching consequences, including but not limited to crop failures, water scarcity, displacement of populations, and increased risks to infrastructure failures (Peters-Lidard et al., 2021; Roy et al., 2022; Zscheischler et al., 2020).

In the summer of 2021, a rare 500-year flood event hit Belgium, Germany, and the Netherlands, resulting in a 3–19% increase in the intensity of maximum 1-day and 2-day rainfall compared to the historical period of 1998–2008 (Kreienkamp et al., 2021). Similarly, the Henan province in China experienced a 500-year flood event in 2021 (Manandhar et al., 2023). The event caused widespread flooding, over 300 fatalities, and damage to infrastructure, agriculture, and transportation systems. According to Khan et al. (2021), the probability of a flood occurring in five years due to projected changes in climate in Pakistan would be 20%, significantly higher than the global average of 2%. Such an event could damage the country's gross domestic product (GDP), amounting to 20.4 billion US dollars (USD), with 8.4 million people at risk and 1.4 billion USD in urban damage.

Over the past few years, numerous regions across the United States (US) have witnessed catastrophic floods. An example of such an event is Hurricane Harvey, Texas, in 2017. The hurricane caused a 500-year flood event, with some locations receiving over 400 mm of rainfall in one day (Hines & Reid, 2020; Yang et al., 2019). Similarly, in 2019, the US Midwest region experienced a 100-year flood. The flooding was caused by rainfall >100 mm/day, leading to several rivers overflowing and causing total damage of around 125 billion USD, making it one of the costliest natural disasters in US history (Swain et al., 2020). According to the Fourth National Climate Assessment Report, heavy precipitation events in the US have increased by approximately 30% in some regions, such as the Northeast, Midwest, and Upper Great Plains, since 1901 (NCA, 2018). The report further estimates that the frequency and intensity of such events will likely increase. For example, by mid-century (2041–2060), approximately 70% of the US Northeast and Midwest regions are projected to drop in precipitation totals (Pal et al., 2023). Marsooli et al. (2019) projected that by the late

21<sup>st</sup> century, the historical 100-year flood could occur annually in New England and mid-Atlantic regions and every 1 to 30 years in the southeast Atlantic and Gulf of Mexico.

Aside from floods, droughts have also become a growing concern globally. According to the World Meteorological Organization (WMO), the regions affected by drought worldwide, such as Australia, Brazil, China, and South Africa, have expanded by 16% in just ten years (from 2011 to 2020), with more than 1.5 billion global population affected by drought-related events (WMO, 2022). The drought that started in 2015 in Cape Town, South Africa, is a specific example that led to water scarcity as the reservoir water levels dropped by more than 70% in just three years (Cole et al., 2021). Between 2012 and 2015, Brazil's south-central region experienced a water level drop in major reservoirs by more than 75%, resulting in critical water shortages for municipal and agricultural sectors (Getirana et al., 2021). The IPCC's sixth assessment report reveals alarming estimates that climate change could result in water scarcity to 40–70% of the global population by 2050, contingent upon greenhouse gas emission trajectories (IPCC, 2021). Furthermore, the report projects that the frequency of drought events in several regions, including southern Africa, the Mediterranean, North America, Europe, and Central Asia, could increase by up to 80% by the end of the 21<sup>st</sup> century (IPCC, 2021). These climate change related projected droughts and water shortages underscore the gravity of the situation and the urgent need to address climate change to mitigate its impact on water resources and their beneficiaries.

Zipper et al. (2021) analyzed streamflow records from 540 gages with at least 30 years of records since 1980 and found an increasing non-perennial condition of streams over most parts of the US and widespread drying in the southern US. Dudely et al. (2020) analyzed the annual 7-day streamflow trend in 2482 gauges in the US between 1916 to 2015 and found

decreasing streamflow trend in most southeastern and northwestern US. According to the National Oceanic and Atmospheric Administration (NOAA), drought-impacted regions in the US have increased in recent years (NOAA, 2020). In the 2000–2020 period, the US experienced 22 events designated as "billion-dollar droughts," which are drought events that caused at least one billion USD in damages each year. Drought conditions are classified based on the severity and duration of the drought. There are four categories of droughts—moderate, severe, extreme, and exceptional based on the order of droughts' severity (Sharma et al., 2022). These categories are based on various factors, including soil moisture content, rainfall deficit, and vegetation health. Between 2000 and 2023, approximately 20–80% of the US land experienced at least moderate drought and up to 25% extreme to exceptional drought (National Drought Mitigation Center, 2023). The extent of the contiguous US experiencing moderate to extreme drought is projected to increase throughout the 21<sup>st</sup> century (IPCC, 2014b; Mbow et al., 2017). Between 2046 and 2065, the central and western regions of the US could experience an increase in the frequency of droughts by 5–20% in the mid-century (2046–2065 period) and by 20–30% in the late century (2081–2100 period) compared to the baseline (1986–2005 period) (IPCC, 2014b; Gamelin et al., 2022). As droughts intensify, water sources such as rivers, creeks, lakes, reservoirs, and wetlands may dry up faster than average, leading to water shortages for natural cycling and human uses, such as households, businesses, agriculture, and industrial activities.

While climate change is altering the terrestrial water cycle and budgets through droughts and floods, urbanization is one of the variables driving both climate change and water demand, with cities accounting for a home to >56% of the global population (He et al., 2021), and >70% of global greenhouse gas emissions (Pee & Pan, 2022; Xian et al., 2022). The global

water demand is estimated to increase by 55% in the 2050s compared to the 2000s; most of the increase is attributed to urbanization and associated infrastructure growth (UN, 2021). Increased urban population growth and economic activities coupled with an increase in drought events lead to reduced surface water flows and limited water availability in the already water-depleted regions such as the Middle East, North Africa, South Asia, and many parts of North America, including southwestern and southern US, prompting unsustainable groundwater mining (Naresh et al., 2021), heightened competition for water resources among various users and sectors, such as agriculture, energy production, and municipal water supplies (Brown et al., 2019), and increased cost of building new infrastructures and maintaining and upgrading existing infrastructures (Leigh & Lee, 2019; McManamay et al., 2019; van Dijk et al., 2020).

In the US, groundwater depletion has become a critical issue impacting water resources and ecosystems. One alarming example is the Central Valley in California, renowned for its agricultural productivity. Since 2019, the rate of groundwater depletion in this region has surpassed that of the previous two droughts by 31%, resulting in a total loss of approximately 4.4 km<sup>3</sup> (~36 million acre-feet). To put this into perspective, it is equivalent to 1.3 times the full water-storing capacity of Lake Mead, the largest reservoir in the US (Los-Angeles-Times, 2022). Similarly, the High Plains Aquifer, including areas in Texas, Kansas, Nebraska, and Colorado, has faced depletion due to unsustainable pumping practices, with an estimated decline of about 30% due to tens of thousands of wells actively pumping water from the Ogallala Aquifer (Perez-Quesada et al., 2020). Over time, this extensive water extraction has led to a significant depletion of the aquifer, with estimates indicating a reduction of around 50% in its water levels. In addition, in response to growing water demand, the construction of new water infrastructure and systems is rising in many areas of the US, including investments

in water treatment and distribution, storage, and conservation. Many cities and towns struggle with aging water distribution systems that exceed their intended lifespan. Studies indicate that approximately 240,000 water main breaks occur each year in the US, resulting in the loss of about 22.7 billion liters (~6 billion gallons) of treated water annually (Galan et al., 2020). According to the American Water Works Association, replacing water pipes over the next few decades to accommodate climate change and urbanization would cost up to one trillion USD (AWWA, 2020). The USEPA estimates an expenditure of >744 billion USD over the next decade on water infrastructure, including pipes, treatment plants, and wastewater management facilities (USEPA, 2022).

The US population growth, particularly urban growth, amplifies the urgency of addressing challenges associated with water resources. Between 2000 and 2022, the US population increased from 281 million to 334 million, representing a significant growth of 18.9% (United States Census Bureau, 2022). This population growth exerts additional pressure on water resources and infrastructure, necessitating proactive measures to meet the increasing water demand and maintain the integrity of aging systems. The current urban water usage in the US is approximately 1,219 billion liters (~322 billion gallons) per day, with around 27% used for outdoor purposes such as irrigation and landscaping (USEPA, 2022). Nonetheless, projections suggest that 2050 urban water usage could increase by 20 to 50% above the current levels.

### **Water Resources and Climate Change in Texas**

The Texas Water Development Board (TWDB) has projected that Texas population will increase by 70% from 29 million to over 51 million between 2020 and 2070 (TWDB, 2022b). As a result, the state's water demand could rise by 22% from 22 billion liters (~5.8

billion gallons) per year in 2020 to over 27 billion gallons (~7.1 billion gallons) per year in 2070. Nearly one-third of this water demand is from urban areas. Texas has approximately 307,385 kilometers (~191,000 miles) of rivers and streams, with surface water contributing 60% of the total water supply. Additionally, nine major and 21 minor aquifers provide around 40% of the total water supply. However, Texas is still at risk of water scarcity, droughts, and floods due to its growing population and the influence of climate change (Makarigakis & Jimenez-Cisneros, 2019). In 2020, Texas faced a water shortage of 5.7 million liters (~1.5 million gallons). However, according to TWDB projections, this number is expected to increase by approximately 87% to 11 million liters (~2.9 million gallons) of water shortage by 2070 (TWDB, 2022b). Therefore, the Texas Senate has recently allocated billions of USD in water conservation, infrastructure development, and research to address these water challenges and ensure a sustainable and resilient water supply for the state's growing demands (Texastribune, 2023).

Climate change has affected and will continue to affect the availability of fresh water in Texas. Between 1895 and 2022, the average rainfall and temperature are increasing, with rainfall increasing by 5 mm (0.2 inches) per decade and temperature by 0.06°C per decade (NOAA 2023). By 2036, Texas's average annual surface temperature is expected to be 1.66°C (~3.0 °F) warmer than the 1950–1999 average. Similarly, the frequency of extreme rain events by 2036 is estimated to rise 30–50% compared to 1950–1999 (Texas-Climate-Summaries, 2022). In 2011, Texas experienced its most severe single-year drought, resulting in agricultural and livestock losses amounting to 7.6 billion USD, 301 million dead trees (equivalent to 6.2% mortality statewide), and the depletion of numerous lakes and rivers (Nielsen-Gammon et al., 2020). Besides surface water, the groundwater source, for example, the Edwards Aquifer in

Texas, is particularly susceptible to climate change due to its shallow depth and high karst permeability; as a result, rapid surface-subsurface connections, considered important for sustained baseflow in many rivers, may slow down (Kloesel et al., 2018). Studies estimated that climate change could trigger a 1.5–3.5% increase in municipal water demand and a 31.3% increase in agricultural irrigation demand, and a 20–30% decrease in groundwater recharge by 2090 in the Edwards region (Loáiciga & Schofield, 2019; Mace, 2019; Sharp Jr et al., 2019). These changes could result in a flow reduction of 10–16% at Comal Springs, the largest spring system in the southwestern US, by 2030 and 20–24% by 2090, leading to estimated regional welfare losses of 2.2–6.8 million USD per year (Guerra & Debbage, 2021).

Over the past few years, the population of the Dallas-Fort Worth (DFW) Metroplex, the largest metropolitan area in Texas, has experienced rapid growth, with a growth rate of approximately 2.1% per year compared to a 1.5% annual growth rate in other regions (United States Census Bureau (2022)). As a result, the DFW metroplex has experienced a population surge of about 25% since 2010. This rapid growth has substantially strained the region's resources, particularly its water supply, as the water demand has increased faster than anticipated. The DFW metroplex is projected to exceed 10 million people in the 2030s, becoming the third-largest metropolitan area in the US, and will add 4 million more people by 2070. Unfortunately, this rapid population growth will only worsen the already-existing water management challenges. As a result, the total water demand in the DFW region could increase by 63% from 3.6 million liters (~0.95 million gallons) in 2020 to 5.7 million liters (~1.5 million gallons) in 2070. Such increases in water demand will increase investment in constructing new reservoirs and retrofitting, expanding or updating aging reservoirs in the region (TWDB, 2022a).

Texas has approximately 6,976 reservoirs, of which about 200 are designated for urban and rural water needs (Little, 2005). The DFW region depends on 25 operational reservoirs, with three additional reservoirs planned to meet future water demand (TWDB, 2022b). These reservoirs support the water needs of the increasing population in different residential, commercial, and industrial sectors. The DFW region has traditionally experienced high-water demand due to its growing population and economic activities. However, recent efforts to promote water conservation have led to a reduction in per capita water use. According to TWDB, the DFW region's per capita water use was approximately 541 liters (143 gallons) per day in 2020, which is lower than the state average of 587 liters (155 gallons) per day (TWDB, 2022b). Therefore, it is crucial to understand how these reservoirs are affected by projected changes in future climatic conditions of the region.

The primary aim of this project is to model how projected changes in future climate would alter water inflow into the Eagle Mountain Lake Reservoir in North Central Texas, USA. To meet this primary objective, this study will develop a hydrological model of the watershed that drains into the Eagle Mountain Reservoir, evaluate the performance of the model using daily streamflow data measured and archived by the US Geological Survey (USGS) at several gauge stations within the watershed and feed the model with different climate change scenarios to quantify the associated effects in streamflow entering the reservoir. This research potentially bridges the existing knowledge gap by quantifying any uncertainties over the hydrological impacts of climate change on the Eagle Mountain Lake Reservoir and providing insights into the appropriate climate change adaptive management strategies useful for reservoir operators, regional water resource managers, concerned stakeholders, planners and policymakers in the region

## CHAPTER II

### REVIEW OF LITERATURE

Several studies have employed hydrological models to study the impacts of climate change on water quantity globally. For example, Erler et al. (2019) assessed the effects of climate change on water resources in the Grand River Watershed, located in the Laurentian Great Lakes region in southern Ontario, Canada. They analyzed high-resolution climate projections from the Weather Research and Forecasting (WRF) model, which simulated precipitation and temperature changes for fifty years (2050–2099). The authors integrated the WRF model with an interactive lake model (FLake) to capture the effect of the Great Lakes on the regional climate. Their simulations found that changes in summer precipitation enormously impacted water availability and streamflow in the Grand River Watershed. Specifically, a 20% reduction in projected summer precipitation led to a 10–15% decrease in streamflow for all seasons except for the spring peak, which remained the same. Conversely, a 20% increase in the projected summer precipitation led to a 10–15% increase in streamflow for all seasons except for the spring peak (Erler et al., 2019).

The study conducted by Pokhrel et al. (2021) used ensemble hydrological simulations to investigate the potential impact of climate change on terrestrial water storage (TWS). Specifically, the study found that TWS could be reduced by 7–8% in the Southern Hemisphere, the US, and southwestern Europe by the end of the 21<sup>st</sup> century, compared to a 3% reduction during the 1976–2005 period. Edamo et al. (2022) examined the impact of climate change on water availability in the Bilate catchment, Southern Ethiopia using projections from five climate models for the baseline (1976–2005), the 2050s, and 2080s climate under two emission scenarios by employing the Hydrologic Engineering Center of Hydrologic Modeling System

(HEC-HMS) model. The authors found an increase in projected temperature (1.1–1.3 °C in the 2050s and 2.2–2.5 °C in the 2080s) and precipitation (5–12% in the 2050s and 4–15% in the 2080s). In addition, they found an increase in the projected streamflow by up to 27% in the 2050s and 25% in the 2080s for all climate models. The study by Li and Fang (2021) assessed the impact of climate change on streamflow in the Mun River Basin in Thailand using the soil and assessment tool (SWAT) model. The study found that monthly average streamflow could increase by 10.5–23.2% in the 2020–2093 period, mainly owing to the projected increase in precipitation in the late century by 8.9–139.9%. On the other hand, Saade et al. (2021) estimated a decrease in the average annual discharge of El Kalb River in Lebanon by 28 to 29% in the 2021–2040 period and by 23–45% in the 2081–2100 period owing to the projected climate change with increased temperature (2.75°C) and decreased average annual rainfall (~41%). Furthermore, Singson et al. (2023) estimated that the streamflow to Magat reservoir in the Philippines would reduce (up to 19%) during dry years and increase (~19%) during wet years due to broader variability in projected rainfall (-35.8% to +48.4%) and temperature (+2.0°C to 2.5°C) in future as compared to the historical climate.

Several studies have investigated climate change's impacts on streamflow on US rivers and creeks. For example, Naz et al. (2018) examined the effect of climate change on streamflow events in 138 headwater subbasins located upstream of reservoirs across the conterminous US (CONUS) under 97 Coupled Model Intercomparison Project Phase 5 (CMIP-5) Global Climate Models (GCMs) under four Representative Concentration Pathways (RCPs)—2.6, 4.5, 6.0, and 8.5 using Variable Infiltration Capacity (VIC) hydrologic model. Their findings indicated an increase in streamflow by an average of 4.5% (2011–2050) compared to the baseline period (1966–2005). However, the majority of subbasins located

upstream of flood control reservoirs in the central US could experience a significant rise in high streamflow of up to 44%, while subbasins situated upstream of hydropower reservoirs in the western US could experience a decrease of 11% in low streamflow. By the mid-21<sup>st</sup> century, the model projections indicate that the average temperature in the CONUS is expected to increase by 0.5–2.0°C compared to the baseline period of 1966–2005 and projected increase in winter precipitation by up to 20%, and overall precipitation projected to remain constant or slightly decrease (Naz et al., 2018). Another study in the middle Rio Grande basin in central New Mexico considered 97 future climate scenarios to assess reservoir operations regarding storage and release and found an 11.4% decline in yearly reservoir release volume in the 2021–2070 period compared to the historical period (1971–2020). This decline in annual reservoir release is associated with a projected rise in temperature by 1.7°C and a drop in annual rainfall by 2 mm (Holmes et al., 2022). Sunde et al. (2017) found reductions in annual streamflow (5.9–26.8%) for the 2040–2069 period in the Hinkson Creek watershed, Missouri, under two CMIP5 climate models which projected change in rainfall by  $\pm 7.6\%$  and increase in average temperature by 0.5–6.6°C.

Several SWAT-based studies indicate varying impacts of climate change on water resources in the US. For example, Ercan et al. (2020) assessed the impact of climate change on the water balance of the Upper Neuse Watershed in North Carolina, which serves as a critical water source for more than 1.5 million people. The authors reported decreased evapotranspiration (5.5–7.6%), leading to increased water yield (25.1–33.2%) in the watershed due to an increase in projected rainfall (7.7–9.8%). The study findings indicated an increase in precipitation of 7.7% from the baseline period (1961–2000) to the mid-century period (2046–2065), and by 9.8% between the baseline and end-century (2081–2099). During the same

periods, evapotranspiration (ET) is projected to decrease by 5.5% and 7.6%, while water yield is expected to increase by 25.1% and 33.2%. On the other hand, under the higher emission scenario, the model results reveal significant seasonal differences. ET is estimated to decrease by up to 42%, and water yield to increase by up to 157% during late summer and fall (Ercan et al., 2020). Borchardt and Choi (2023) simulated the cumulative impact of climate change and high-capacity well pumping on groundwater levels and streamflow in Northeastern Wisconsin using an integrated SWAT-MODFLOW modeling platform. They estimated that a 5% increase in annual precipitation would lead to a 16.7% increase in groundwater recharge and a 14.1% increase in streamflow. However, the projected increase in average yearly temperature by approximately 3°C would result in a net deficit in streamflow (-23.4%) and groundwater recharge (-19.6%) in Northeastern Wisconsin.

Tefera and Ray (2023) assessed the impact of future climate change scenarios on hydrology and hydrological extremes using SWAT in the Bosque watershed, North-Central Texas. The simulations revealed a decrease (up to 9.1%) or increase (up to 4.9%) in precipitation and a consistent increase in maximum temperature ranging from 0.34°C to 4.10°C, and minimum temperature ranging from -0.15°C to 3.7°C, in different climate model simulations. These projected rainfall and temperature changes from 2031 to 2099 could decrease the mean annual streamflow by up to 89%. Using SWAT, Chen et al. (2021) assessed the impact of climate change on water footprints and crop production in the Palo Duro watershed of the Texas High Plains. The study utilized climate projections from 11 GCMs under four emission scenarios of RCP 2.6, 4.5, 6.0, and 8.5 for mid-century (2040–2069) and late-century (2070–2099). The study found that all 11 GCMs predicted reductions in future irrigation by 63%, crop evapotranspiration by 34%, and crop yields by 13% for irrigated

summer crops of corn and sorghum under RCP 8.5 compared to the baseline period of 1970–1999.

## **CHAPTER III**

### **METHODOLOGY**

#### **Study Area**

Zhang et al. (2020) highlight that Eagle Mountain Lake, one of the water-supply reservoirs and recreational areas in the DFW metroplex, faces a significant challenge in meeting water demand from the growing population and major water-intensive industries in the DFW metroplex. Furthermore, Melosi (2021) noted that conflicts have arisen among stakeholders, such as cities, industries, and farmers, over the allocation of shrinking water resources amid increased needs. Despite the potential impacts of climate change affecting water resources in the region, to the best of our knowledge, no scientific research has investigated potential climate change's effects on the hydrology of Eagle Mountain Lake.

The lake is situated at the lowest elevation of the Upper West Fork Trinity watershed (Figure 3.1), a fourth-level sub-basin with an 8-digit Hydrologic Unit Code (HUC) of 12030101. The watershed covers an area of 3,547 km<sup>2</sup> (~1,370 mi<sup>2</sup>) and exhibits an average elevation of 255 meters (ranging from 456 meters upstream to 201 meters downstream),

flowing towards Eagle Mountain Lake. As of 2021, approximately 37,000 individuals reside within the watershed (West-Fork-Demographics, 2021). The USGS measures the streamflow in the Upper West Fork Watershed at four gauging stations (Figure 1). The current dominant land uses/land covers in the watershed are pasture/agriculture (65%), forest (18%), urban (9%), and other land uses (8%) (Bariamis & Baltas, 2021). The watershed has a humid subtropical climate, with hot summers and mild winters as per the Koppen-Geiger climate classification (Beck et al., 2018). The long-term average annual temperature ranges from 16.7°C to 18.3°C, and the average annual precipitation is approximately 508 mm (~20 inches). The Tarrant Regional Water District (TRWD) regularly monitors the lake's water level. As of March, 2024, it was reported to be approximately 196.3 m (~644 ft) above the mean sea level (AMSL), which is 77% of the reservoir capacity. However, the reservoir has fluctuated between 194.5 m to 200.2 m AMSL between 1990 to 2024. During the 2010 – 2015 drought period in Texas, the reservoir was hovering at 50% capacity (Chauhan et al., 2020; TRWD, 2023); Texas Water Development Board [TWDB], n.d.).

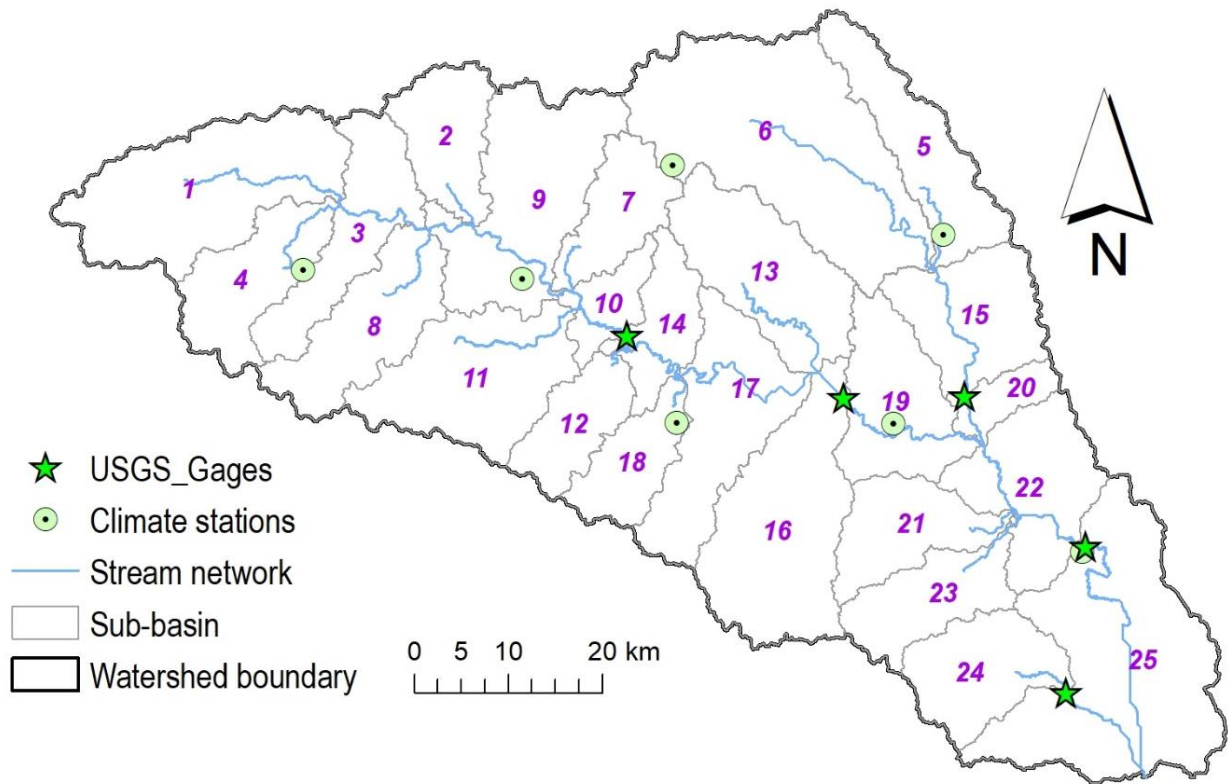


Figure 3.1 The Upper West Fork Trinity Watershed with major land cover and streamflow stations

The Eagle Mountain reservoir plays a crucial role as a water supply source for the Region C area (Figure 3.2), one of the 16 regional water planning groups in Texas, comprising 16 counties. TWDB and TRWD oversee the management of the region's water supply needs, ensuring a reliable and sustainable water source to support the area's growing population and economy. TRWD (2023) reported that Eagle Mountain Lake provides drinking water to over 400,000 residents in North Texas and accounts for approximately 5% of the total water supply for the region. In addition to its significance as a water supply source, the lake is a popular recreational destination for activities such as fishing, boating, and other water sports generating an estimated annual revenue of 1.7 million USD (Eagle-Mountain-Revenue, 2022).

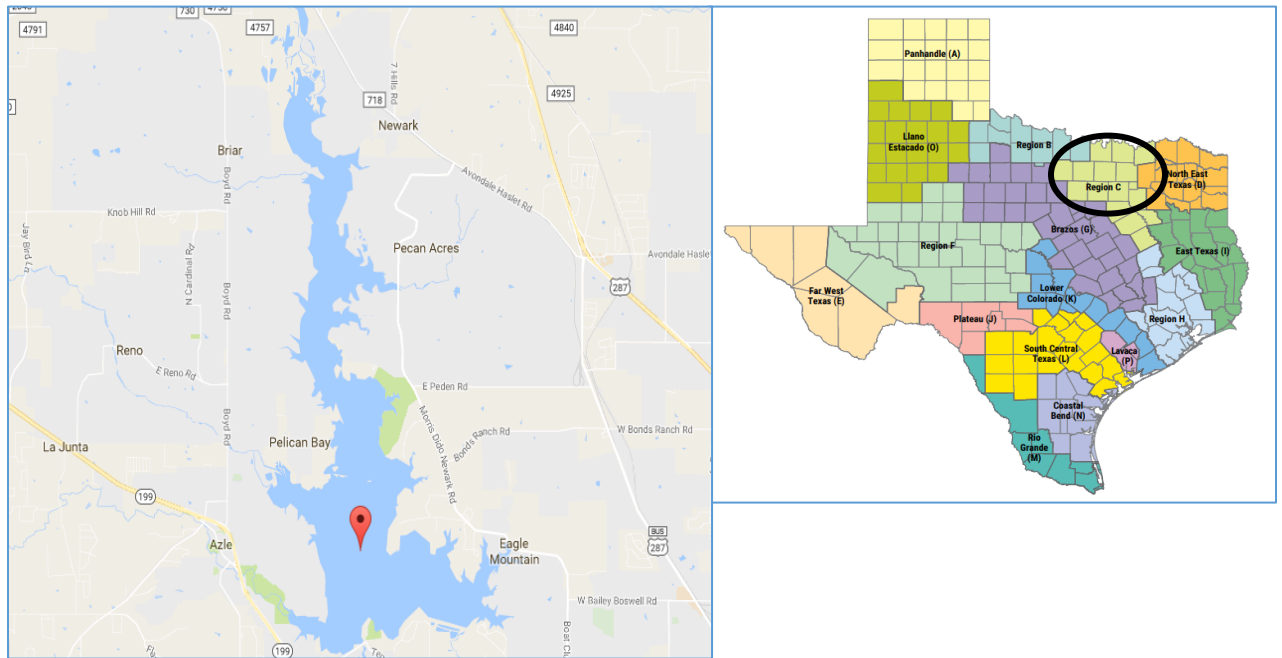


Figure 3.2 Eagle Mountain Lake located in Region C (black circle in the map), North Texas area (Source: TWDB, 2022b; Eagle-Mountain-guide, 2017).

A hydrological model of the study area was developed using the Soil and Water Assessment Tool (SWAT) modeling platform. SWAT is one of the most popularly used hydrological models developed by Arnold et al. (1998). The SWAT model is a semi-distributed, physically based model used to simulate the effects of various land use, climate, and management practices on the water balance of a watershed. It considers the interactions between various hydrological cycle components, including precipitation, evaporation, infiltration, and runoff (Rossetto et al., 2019). This model provides a detailed representation of the water balance at a watershed scale, making it a valuable tool for researchers and water resource managers. The model comprises several modules representing different processes such as infiltration, sub-surface flow, surface runoff, groundwater recharge, and crop growth. It also includes customizable databases of weather, soil, and land use information to represent

specific watersheds (Kang et al., 2022; Zhang et al., 2022). In addition, the model can run on a daily or sub-daily time step and simulate long-term water quality and quantity changes under different land management and climate scenarios. Using historical and projected climate data, the model can estimate the impacts of climate change on water resources, including changes in streamflow, groundwater recharge, and water quality (Zhao et al., 2022). The SWAT modeling platform is integrated within a geographic information system (GIS), which enables the incorporation of different geospatial data such as soil, land cover, climate, and topographic features. It is available as a plugin to the ArcGIS interface called ArcSWAT.

The watershed water balance is the key driving force behind all watershed processes in SWAT (Mishra et al., 2017). The water balance in any modeled watershed involves determining the volume of water entering the watershed and tracking the water flow to its destination or outlets. The water balance equation (Eq. 1) represents the hydrologic cycle in the SWAT model, considering the surface and sub-surface hydrology above the impermeable layer as a single unit.

$$SW_t = SW_0 + \sum_{t=1}^t (P_{day} - Q_{surf} - ET_a - W_{seep} - Q_{gw}) \quad (1)$$

Where  $SW_t$  = final soil water content;  $SW_0$  = initial soil water content;  $P_{day}$  = amount of precipitation per day;  $Q_{surf}$  = surface runoff daily;  $ET_a$  = amount of evapotranspiration daily;  $W_{seep}$  = quantity of water seeping into the soil;  $Q_{gw}$  = amount of return flow per day.

## Watershed Data for SWAT Model

In developing the SWAT-based hydrological model for this research, acquiring and preparing essential data is important. Various datasets, including the digital elevation model (DEM), a land-use map, a soil map, and weather variables, were required to construct the model. Table 3.1 presented below, enumerates the data that was gathered and utilized in the construction of the SWAT-based model for the study watershed.

Table 3.1. Input data and their sources for developing the hydrological model of the watershed

<b>Data type</b>	<b>Description</b>	<b>Resolution</b>	<b>Source</b>
Topography and slope	Based on the Digital Elevation Model (DEM)	10 meters	The United States Geological Survey (USGS)
Land use and land cover	Land-use classification	30 meters	National Land Cover Dataset from USGS
Soil	Gridded Soil Survey Geographic (gSSURGO) database	County-level, reclassified to 30 meters	The United States Department of Agriculture (USDA)
Climate	Daily precipitation, minimum temperature, and maximum temperature for seven stations	Daily	The National Oceanic and Atmospheric Administration (NOAA) and PRISM climate group

## Topographic Information

A 10-meter digital elevation model (DEM) was acquired from the United States Geological Survey. The downloaded DEM had a larger coverage than the study watershed. Consequently, additional processing was necessary, including the application of a 5-kilometer buffer and cropping to the watershed extent using geoprocessing tools in ArcGIS Pro. These operations were performed using a shapefile representing the Upper West Fork watershed. Figure 3.1 illustrates the resulting elevation variations (180.56 m to 463.60 m) within the watershed, with dark orange/red representing higher elevations and yellow to dark green indicating medium to lower elevations.

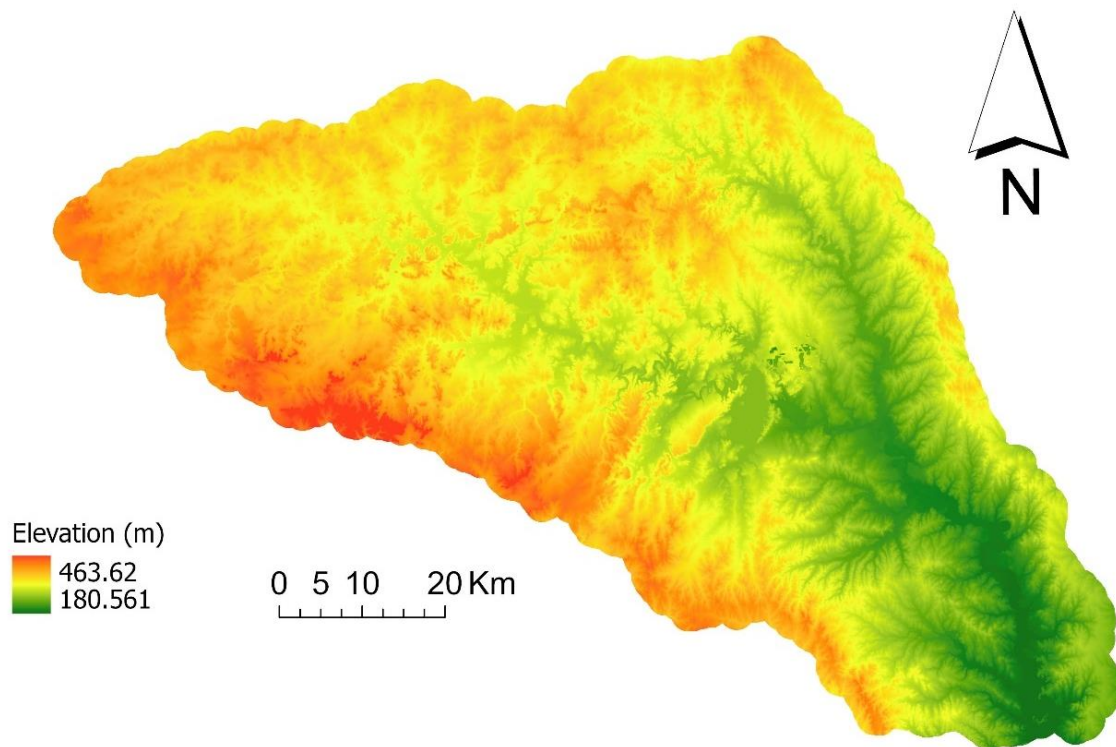


Figure 3.3. Elevation gradient in the study watershed

## **Land Use and Land Cover**

Land use data was obtained from the land-use crop layer of year 2016 (USDA-National Agricultural Statistics Cropland Data Layer, 2016). The NLCD comprised of 16 land classes based on a modified Anderson Level II classification system (Homer et al., 2020). For the specific objectives of the study, the NLCD dataset was refined. The initial sixteen land classes were combined into a more concise set of eight broader categories. This consolidation was accomplished by merging related and smaller land areas (for example, evergreen and deciduous forests were combined into one forest class) to ensure that the reclassified categories better aligned with the actual land cover within the watershed. The resulting eight classes are as follows: agricultural land, barren land, forests, urban areas, grass/pasture, wetlands, open water bodies, and shrubland.

## **Soil Data**

Soil information within the watershed was sourced from the soil survey geographic database—SSURGO (USDA, 2020). The SSURGO datasets contain a comprehensive collection of map data and information about soil properties. These datasets are created for specific soil survey areas, such as a single county or parts of multiple counties. The maps in SSURGO have different scales, ranging from 1:12,000 to 1:63,360. Larger scales provide more detailed information. The primary goal of SSURGO mapping is to support natural resource planning and management for landowners, townships, and counties. Understanding the nuances of soil data and map scales is important to avoid misunderstandings. The maps in the database are linked to details about the component soils and their properties for each map unit. Each map unit typically contains one to three major and several minor components. Soils are categorized into four hydrologic soil groups based on their ability to infiltrate water (Table 3.2). Hydrologic

soil groups are essential for hydrological modeling, as they provide a simplified method to estimate a soil's potential for runoff and infiltration. Hydrological models such as SWAT simulate water movement through a watershed, including infiltration into the soil, surface runoff, and groundwater recharge. Infiltration capacity is critical in determining how much water can seep into the ground and how much will flow over the surface as runoff.

Table 3.2. Description of Hydrologic Soil Groups (HSG) (USDA, 2020)

Hydrologic Soil Groups	Soil Texture	Runoff Potential & infiltration rates (cm/hr)	Remarks
A	Sand, loamy sand, or Sandy loam: deep, well-drained sands and gravel	Low (>7.6)	High rate of water infiltration; useful in flood control and aquifer recharge; infiltration rates (>7.6 cm/hr)
B	Silt loam or loam: moderately deep, well-drained with moderately fine to coarse textures	Moderate (3.8 to 7.6)	Moderate rate of water infiltration; balance between infiltration and runoff; infiltration rates (3.8 to 7.6 cm/hr)

C	Sandy clay loam, shallow sandy loam, soils with moderately fine to fine textures	Moderate (1.3 to 3.8)	Moderate rate of water infiltration; increased surface runoff potential; infiltration rates (1.3 to 3.8 cm/hr)
D	Clay loam, silty clay loam, sandy clay, clay soils that swell significantly when wet, heavy plastic and soils with a permanent high-water table	High (<1.3)	Low rate of water infiltration; increased risk of flooding and erosion; infiltration rates (<1.3 cm/hr)

### **Climate Data**

Climatic data, including average daily precipitation, average daily minimum temperature, and average daily maximum temperature, for the watershed were obtained for seven weather stations (Figure 3.1) detailed in Table 3.3, accessible through NOAA's climate data online portal (NOAA, 2020) and the PRISM Climate Group. A selection process was undertaken to identify these seven weather stations based on criteria such as daily data availability within the watershed, data availability for a time span of at least 30 years of model simulation (from 1990 to 2022), and sufficient data coverage (e.g., continuous data or no data gaps). The objective of this selection was to identify stations representing the climatic conditions of the watershed, and capable of providing comprehensive and reliable climate data to facilitate the analysis and assessment of climate patterns and trends within the study area. The data collected from these

seven weather stations underwent conversion into the SWAT-acceptable data format and were subsequently integrated into the model.

Table 3.3. Climate Stations used in the Upper West Fork Watershed Model

Station Name	Latitude	Longitude	Source
Alvord, TX	33.39	-97.72	NOAA
Boyd, TX	33.08	-97.56	
Bridgeport, TX	33.10	-97.92	
Markley, TX	33.35	-98.48	
Newport, TX	33.45	-98.02	
Prism 1	33.34	-98.19	PRISM Climate Group
Prism 2	33.20	-98.02	

### Streamflow Data

Streamflow data for 1990 through 2022 within the watershed were obtained from the five USGS stations located in the watershed (Table 3.4). These USGS streamflow gaging stations represent different drainage areas of the watershed, as represented by sub-basins in the SWAT model (Table 3.4). While SWAT does not use these streamflow data as input in calculations, these datasets are used for calibrating and validating the model by comparing SWAT simulated

and USGS observed values. Depending on the availability, the streamflow data of varying lengths were used for model calibration and validation at different USGS gaging locations (Table 3.4). Of the five gaging stations, the station near Boyd, Texas (USGS 08044500) represents the majority of the watershed and it feeds the Eagle Mountain Reservoir.

Table 3.4. Streamflow gauge stations used in the Upper West Fork Watershed model

<b>Station ID</b>	<b>Station Name</b>	<b>Latitude</b>	<b>Longitude</b>	<b>Drainage area (km<sup>2</sup>)</b>	<b>Data availability Period</b>	<b>Sub-basins draining to the gaging Station</b>
USGS 08042800	W Fk Trinity Rv nr Jacksboro, TX	33.29	-98.07	1,770	1956–2023 streamflow	1, 2, 3, 4, 7, 8, 9, 10, 11
USGS 08044000	Big Sandy Ck nr Bridgeport, TX	33.23	-97.69	862	1936–2023 streamflow	5, 6, 15

USGS 08043000	Bridgeport Res abv Bridgeport, TX	33.22	-97.83	2,878	2000-2023	16 (reservoir) <b>10</b> (1, 2, 3, 4, 7, 8, 9, 11), 12, 13, 14, 17, 18
USGS 08044500	W Fk Trinity Rv nr Boyd, TX	33.08	-97.55	4,462	1947-2023 streamflow	22 (main inlet to Eagle Mountain Reservoir) 19,20,21,23, <b>15</b> , 5, 6, 16, <b>10</b> ,1, 2, 3, 4, 7, 8, 9, 11, 12, 13, 14, 17, 18
USGS 08044800	Walnut Ck at Reno, TX	32.94	-97.58	196	1995-2023	24 (small sub-basin feeding into the Eagle Mountain Reservoir)

Note: Eagle Mountain Reservoir above Fort Worth, TX (USGS 08045000) and Bridgeport Reservoir above Bridgeport, TX (USGS 08043000) possess data related to the storage and elevation of the reservoirs. Additionally, the streamflow data for Big Sandy Creek near Bridgeport, TX (USGS 08044000), exhibits a gap, specifically from September 30, 1995, to September 30, 2004, where the data is missing.

### **SWAT Model Setup**

The SWAT model setup for this study involved using ArcSWAT, an ArcGIS-ArcView extension and interface, to facilitate model simulations of all the processes within the SWAT. The version of the ArcSWAT was 2012.10.8.26, which is compatible with ArcGIS 10.8, and loaded with SWAT executable 687 (<https://swat.tamu.edu/software/arcswat/>). The model setup process is illustrated in Figure 4.3, which depicts a flowchart of the SWAT model providing a visual representation of input integration and simulation output.

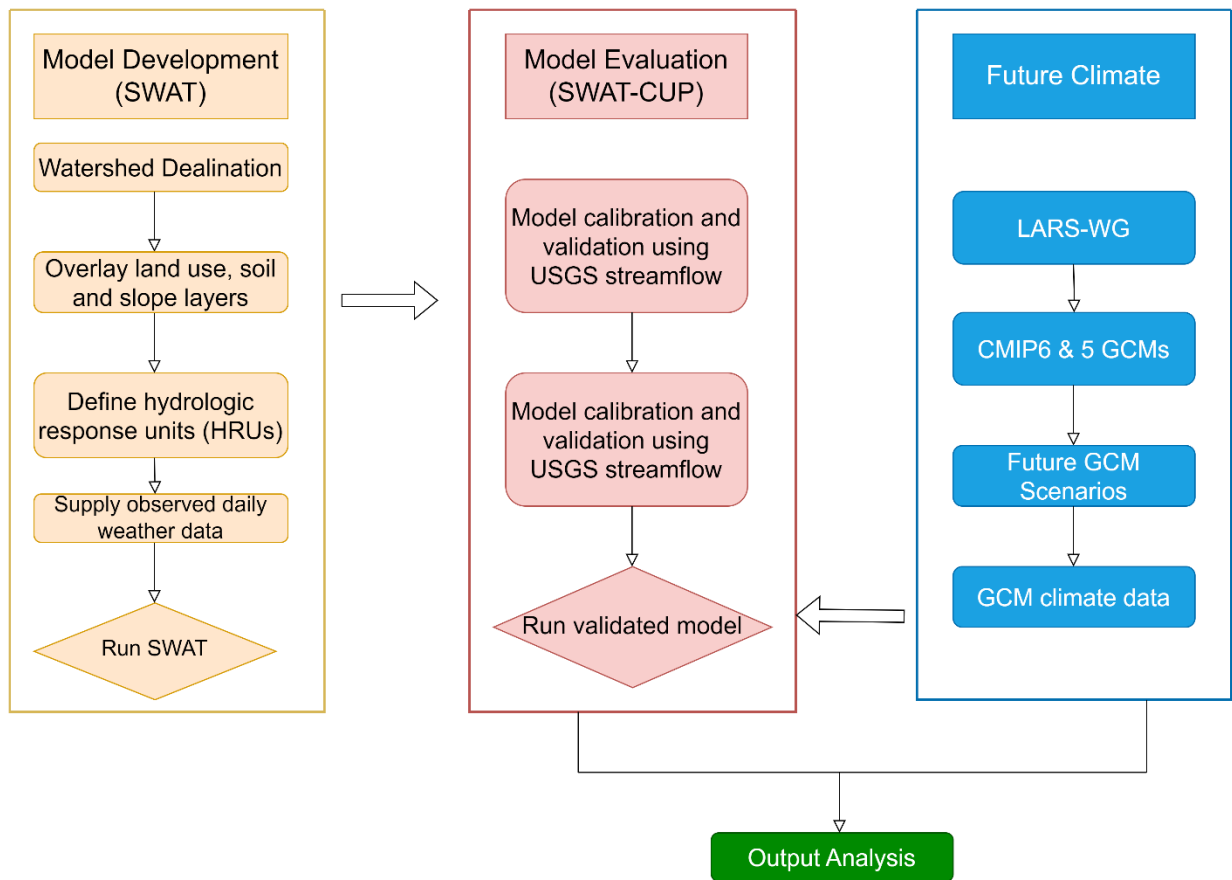


Figure 3.4. Flowchart illustrating the research methodology employed to assess the impacts of climate change on the study watershed hydrology using soil and water assessment tool (SWAT).

### Watershed Delineation

The initial step in the process involved delineating the study watershed and dividing it into multiple sub-basins. This delineation process considered various topographic parameters, including overland slope, slope length, flow direction, and rate of flow for each sub-basin (Swain et al., 2022). To achieve this, a 10-meter Digital Elevation Model (DEM) was uploaded in ArcSWAT interface with the projection of NAD\_1983\_UTM\_Zone\_16N. In the DEM

setup, flow direction and flow accumulation were determined, with numerous DEM pixels or cells set within the range of the watershed area. After adding the minimum drainage area in-stream definition, the stream network within the watershed was created along with junctions or pouring points or confluence of those stream segments and stream network attributes (e.g., river segment length, width, depth, slope, etc.). This process led to creating 25 distinct sub-basins for the entire study watershed, as illustrated in Figure 3.1.

### **Hydrological Response Unit processing**

After delineating the watershed, the next step in SWAT is to process the Hydrologic Response Units (HRUs), which are the unique combinations of homogeneous land-use class, soil types, and slope classes. The delineation of HRUs was based on the overlay of three map layers: LULC map, soil types, and slope classes within each sub-basin. In this step, the LULC map and soil data were loaded. The loaded land use data was 100% overlapped with the DEM (Figure 3.4) to ensure that there are no missing land classes while generating HRUs. A report detailing the percentage of each land use type was generated. The reclassified land cover types for the study watershed model included pasture and agriculture (65%), forest (18%), urban (9%), and other land uses (8%).

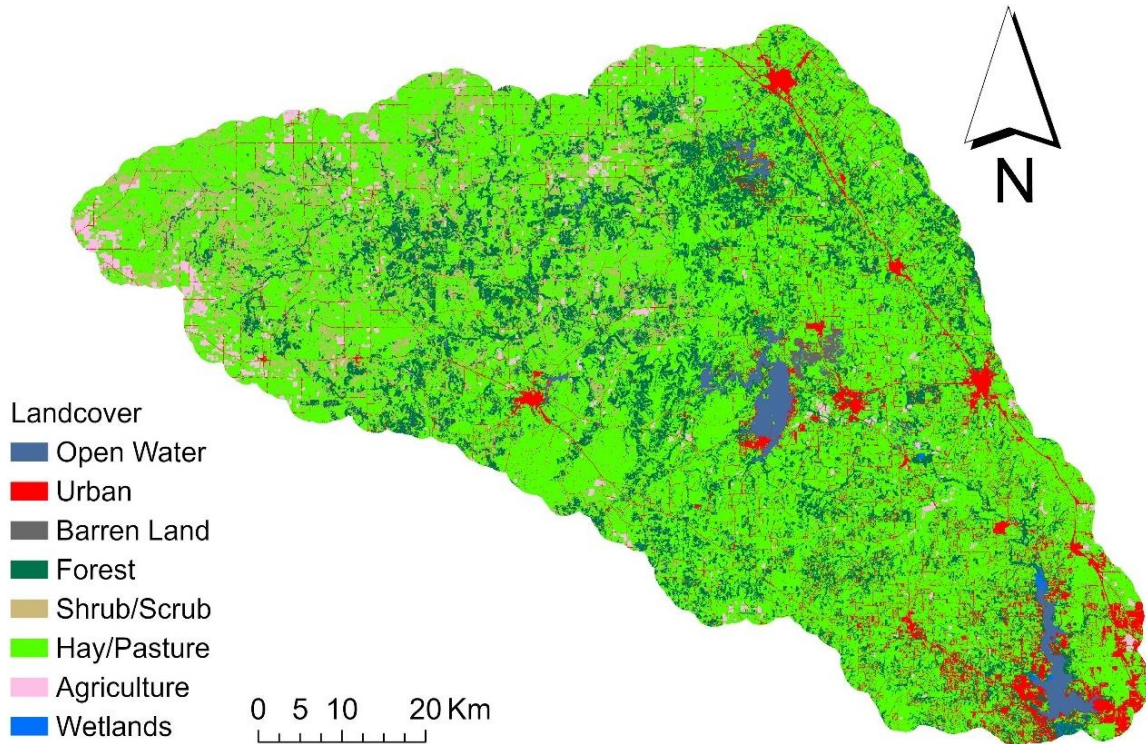


Figure 3.4. Reclassified land use and land cover types in the study watershed

Next, the soil map was overlapped with the DEM and land map by 100% with the study watershed (Figure 3.5). The SWAT model accepts three types of soil data, which are SSURGO, STATSGO and User defined soil types. SSURGO soil data was used for this study.

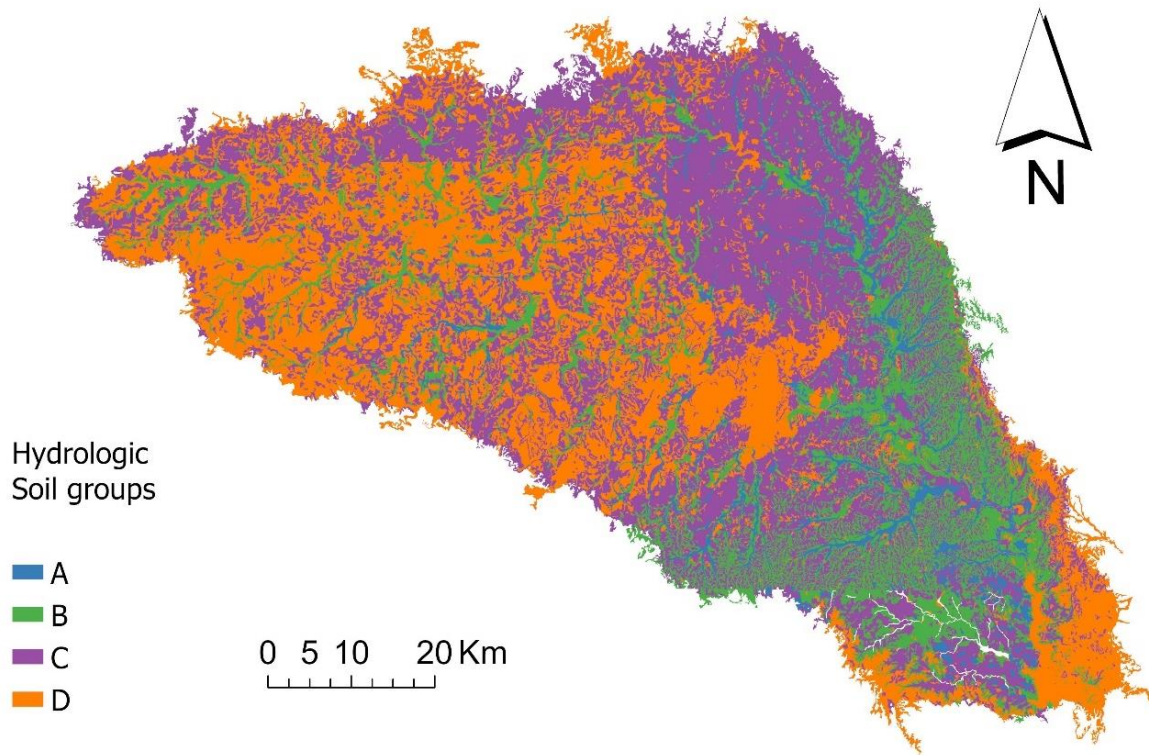


Figure 3.5. Soil hydrologic groups in the study watershed

The next step in the HRU definition process involved introducing slope classes. Slope classification is important to understand the interaction of water with the land surface. SWAT considers slope class in defining water flow velocity in streams, simulating water movement within the channel network, and estimating soil erosion and sediment yield. For this study, the three slope classes were used: slope <2%, slope 2 – 5%, and slope >5% (Figure 3.6). The land use map, soil map, and slope map were overlaid to create 2,118 HRUs for the study watershed.

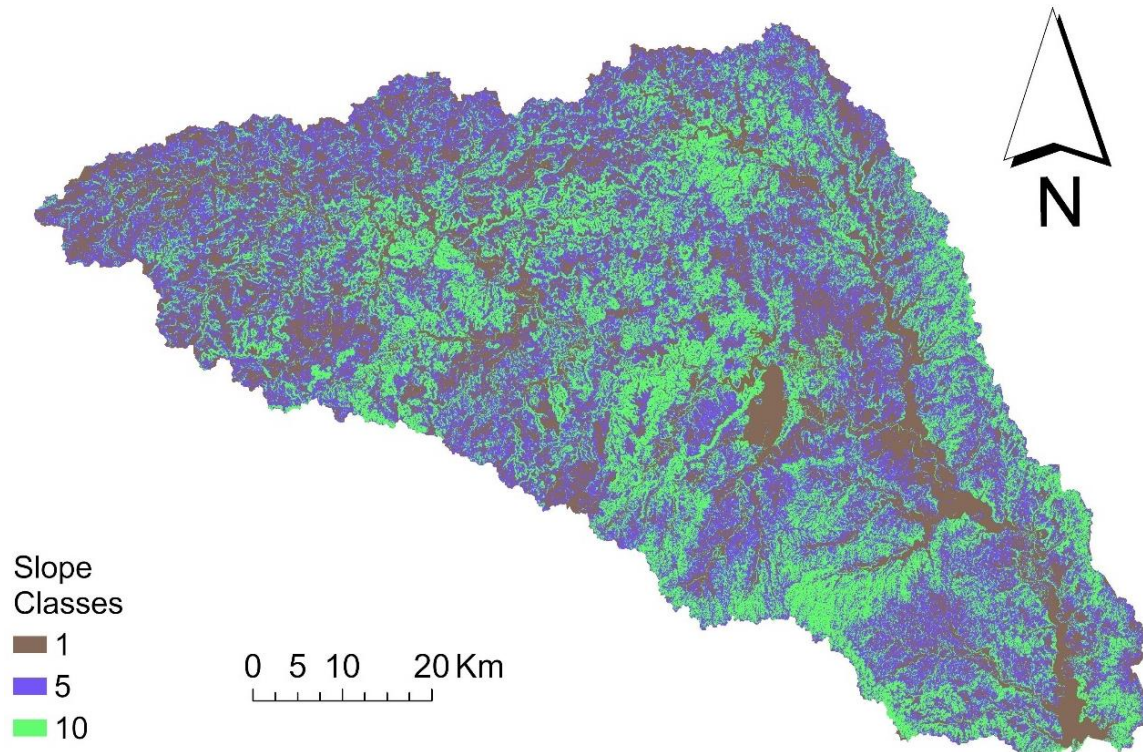


Figure 3.6. Slope classes in percentage in the study watershed

### Writing Input Data Table

The subsequent step in the SWAT model involved loading the weather data, which comprises essential climatic variables such as daily precipitation, maximum/minimum temperature, relative humidity, solar radiation, and wind speed depending on data availability and the type of evapotranspiration method used. Climate data plays a crucial role in SWAT analysis as it influences energy and moisture, regulating the water balance of the watershed (Neitsch et al., 2011; Nyatuame et al., 2020). These data can be sourced by users from historical records or generated using the weather generator integrated into SWAT. The weather generator function in ArcSWAT proves invaluable for filling in missing data or generating information for variables not directly measured in the watershed. Users have two options for utilizing weather data: they can either load observed data from specific meteorological stations within the

watershed or use the synthetic climate data from the inbuilt weather generator. For this study, daily precipitation and daily maximum temperature, and daily minimum temperature data spanning from 1990 to 2022 (Table 3.3) were used.

### **SWAT Model Run**

The SWAT model was run daily for a 33-year period (1990 – 2022). A three-year model warm-up period (NYSKIP) was incorporated into the model setup, allowing the simulation period to commence from 1993. This initial three-year model warm-up period provides the model with the necessary time to establish a consistent streamflow for the 30-year period of interest, ensuring model equilibrium and minimizing the impact of initial conditions on the model output. Following the warm-up period, the SWAT model was configured and made ready for execution (Figure 3.7). The next step involved running the model, which produced output tables encompassing different processes at the HRU, sub-basin, and the watershed or basin levels. The SWAT model outputs represent water quantity, water quality, and plant biomass at HRU, sub-basin, or the basin level. The SWAT output files were saved as text files and MS Access tables.

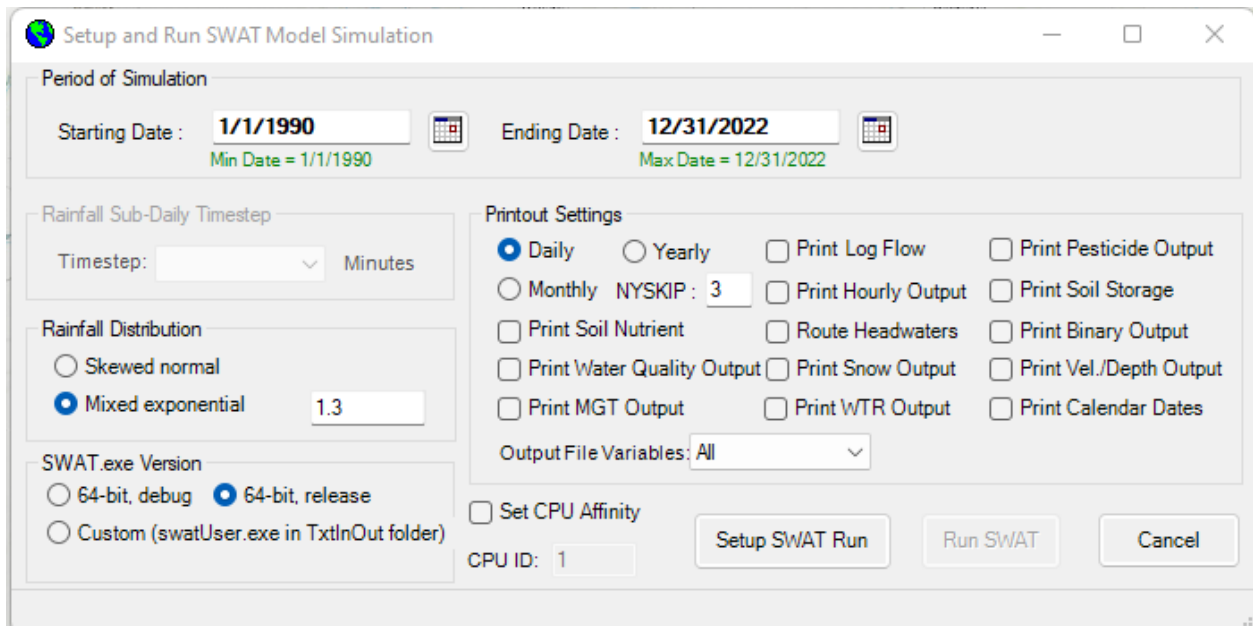


Figure 3.7. SWAT model simulation setup

### SWAT Model Calibration, Validation, and Sensitivity Analysis

Calibration and validation are fundamental steps in the development and application of hydrological models, playing a crucial role in ensuring the accuracy and precision of model predictions. Calibration involves adjusting specific parameters within the model to optimize the agreement between simulated outputs and observed data. Validation, on the other hand, verifies the suitability of the calibrated model parameters for different time periods by reproducing measured observations. These processes are essential to the credibility and reliability of hydrological modeling outcomes. SWAT-CUP Premium tool developed by Abbaspour et al. (2015) was employed for the calibration and validation of this model. SWAT-CUP Premium is a software program designed to calibrate, validate, and enhance SWAT analysis results using various algorithms such as Swat Parameter Estimator (SPE), generalized likelihood uncertainty estimation (GLUE), sequential uncertainty fitting (SUFI-2), parameter solution (ParaSol), and Markov chain Monte Carlo (MCMC) (Kim et al., 2022). In this study,

the SPE method, specifically employing "stochastic calibration," was utilized. SPE is a powerful algorithm capable of addressing uncertainties in the model calibration process. Unlike traditional calibration methods, SPE recognizes and quantifies errors and uncertainties, acknowledging that calibration devoid of considering uncertainty can lead to misleading results. The incorporation of SPE ensures a more robust and meaningful calibration process (Badora et al., 2022; Vagheei et al., 2022).

The initial step in calibrating the watershed model using SWAT-CUP Premium is to identify sensitive parameters. In this case, we selected 22 parameters for model calibration (as shown in Table 3.4). These particular parameters were chosen following an extensive review of relevant literature on SWAT-CUP calibration (Hosseini & Khaleghi, 2020; Malik et al., 2022; Singh et al., 2013; Yu et al., 2020; Yuan & Forshay, 2022). These studies highlighted these parameters as crucial for hydrological modeling within the context of SWAT. Six sub-basins (10, 15, 22, 24, 25, 16), as depicted in Table 3.2, are interconnected, draining into each other. Calibration was conducted separately for each sub-basin to enhance the accuracy of estimating the streamflow entering the Eagle Mountain Lake reservoir.

A multiple regression method with Latin hypercube samples was used to measure the sensitivities of various parameters with respect to the objective function. This global sensitivity analysis was carried out utilizing the specialized capabilities of the SWAT-CUP Premium (Abbaspour et al. in 2007). Statistical measures such as the t-test and p-value were used to ascertain the significance of parameter sensitivity. These tests provide valuable insights into the influence of each parameter on the model's performance (Ben Saad et al., 2023). In the process of parameter ranking based on sensitivity, the parameters exhibiting high sensitivity are characterized by both high absolute t-statistics, whether positive or negative, and the lowest

p-values. A substantial positive t-statistic signifies a parameter's positive impact on the model output, while a significant negative t-statistic indicates its negative impact (de Oliveira Serrão et al., 2022). Concurrently, a lower p-value underscores the parameter's enhanced significance, emphasizing its profound influence on the model (Khalid et al., 2016). By referring to Table 3.4, which presents our parameter sensitivity findings, we identified five distinct parameters that emerge as the most sensitive. These parameters include CN2, ESCO, GW\_REVAP, and GW\_DELAY. Their prominence in the ranking underscores their substantial influence on the model's performance and highlights their pivotal role in shaping the model outcomes.

Table 3.5. A list of model parameters and their sensitivities to streamflow in the study watershed

Parameter Name	t-Stat	P-Value	Ranking
r__CH_S1.sub_____1,2,3,4,7,8,9,10,11	-0.087	0.931	22
v__GWHT.gw_____1,2,3,4,7,8,9,10,11	-0.165	0.869	21
v__CH_N2.rte_____1,2,3,4,7,8,9,10,11	-0.191	0.849	20
v__DEEPST.gw_____1,2,3,4,7,8,9,10,11	-0.253	0.800	19
v__RCHRG_DP.gw_____1,2,3,4,7,8,9,10,11	0.274	0.784	18
r__HRU_SLP.hru_____1,2,3,4,7,8,9,10,11	-0.385	0.700	17
v__CH_K1.sub_____1,2,3,4,7,8,9,10,11	0.392	0.695	16
v__CH_N1.sub_____1,2,3,4,7,8,9,10,11	-0.398	0.691	15
r__OV_N.hru_____1,2,3,4,7,8,9,10,11	-0.413	0.680	14
v__GWQMN.gw_____1,2,3,4,7,8,9,10,11	-0.466	0.641	13
r__SLSUBBSN.hru_____1,2,3,4,7,8,9,10,11	0.786	0.433	12
v__SURLAG.hru_____1,2,3,4,7,8,9,10,11	1.009	0.314	11

r__CH_K2.rte_____1,2,3,4,7,8,9,10,11	-1.260	0.208	10
v__REVAPMN.gw_____1,2,3,4,7,8,9,10,11	1.301	0.194	9
v__SHALLST.gw_____1,2,3,4,7,8,9,10,11	-1.339	0.181	8
v__ALPHA_BF.gw_____1,2,3,4,7,8,9,10,11	-1.484	0.139	7
v__ALPHA_BNK.rte_____1,2,3,4,7,8,9,10,11	1.558	0.120	6
v__EPCO.hru_____1,2,3,4,7,8,9,10,11	1.755	0.080	5
v__GW_DELAY.gw_____1,2,3,4,7,8,9,10,11	-2.006	0.045	4
v__GW_REVAP.gw_____1,2,3,4,7,8,9,10,11	2.695	0.007	3
v__ESCO.hru_____1,2,3,4,7,8,9,10,11	-7.530	0.000	2
r__CN2.mgt_____1,2,3,4,7,8,9,10,11	-30.537	0.000	1

### Sub-basin 10

Following the sensitivity analysis that identified 22 key parameters, the model underwent calibration using monthly observed streamflow data over an 18-year period (1990-2007) for the Sub-basin 10-West Fork Trinity River near Jacksboro, TX (USGS #08042800). The calibration phase, which included a 3-year warm-up period from 1990 to 1992, aimed to optimize the model's performance. Subsequently, the calibrated model was validated using data spanning from 2005 to 2022, incorporating a warm-up period of 3 years from 2005 to 2007. To fine-tune the model further, SWAT-CUP was employed with absolute initial values (Table 3.5). The SWAT-CUP iteratively executed 500 simulations, each time providing new minimum and maximum parameter values. There were four iterations with 500 simulations in each iteration. This allowed users to observe and adjust the evolving parameter range based on suggested values in each iteration. The iterative process continued until a satisfactory parameter range (fitted value) was achieved. To expedite the calibration process, a parallel

processing module was employed. The validation phase followed a similar procedure, utilizing the already calibrated parameters without the need for further iterations, as each iteration encompassed a complete calibration process with 2,000 simulations. It is important to note that the flow of sub-basin 10 was influenced by contributions from eight adjacent sub-basins (1, 2, 3, 4, 7, 8, 9, and 11) (Table 3.2).

Table 3.6. Calibrated parameters for the West Fork Trinity River near Jacksboro, Texas (Sub-basin 10)

Parameters	Fitted value	Minimum value	Maximum value
V_SHALLST.gw	804.839	534.000	1895.000
V_DEEPST.gw	6923.600	3364.000	7764.000
V_GW_DELAY.gw	85.628	9.800	127.000
V_ALPHA_BF.gw	0.264	0.000	0.290
V_GWQMN.gw	618.460	0.000	2140.000
V_GW_REVAP.gw	0.133	0.100	0.150
V_REVAPMN.gw	592.336	501.000	893.000
V_RCHRG_DP.gw	0.022	0.000	0.230
V_GWHT.gw	24.459	20.000	33.000
R_CN2.mgt	-0.155	-0.220	-0.040
V_CH_N2.rte	0.026	0.000	0.100
R_CH_K2.rte	0.253	0.086	0.270
V_ALPHA_BNK.rte	0.439	0.210	0.490
R_SLSUBBSN.hru	0.219	0.060	0.260

R__HRU_SLP.hru	0.118	-0.070	0.240
R__OV_N.hru	0.064	0.057	0.190
V__ESCO.hru	0.135	0.000	0.200
V__EPCO.hru	0.528	0.320	0.640
V__SURLAG.hru	9.529	6.200	13.180
R__CH_S1.sub	-0.344	-0.550	-0.300
V__CH_K1.sub	3.021	1.760	3.430
V__CH_N1.sub	0.026	0.024	0.045

The SWAT-CUP process relies on a parameter identifier to derive adjusted values for fitted parameters. In this context, parameters labeled with "R\_\_" indicate that an existing parameter value is to be multiplied by (1 + a fitted value), "V\_\_" signifies that the existing parameter value is to be replaced by the fitted value, and "A\_\_" implies that the fitted value is to be added to the existing parameter value. For example, referring to Table 3.5, the final CN2 value in the study watershed was adjusted to -0.155, i.e., the default CN2 value was multiplied by 0.845 (1-0.155).

### **Sub-basin 15**

The sub-basin 15 is drained by sub-basins 5 and 6. The calibration process for sub-basin 15 spanned a 12-year period from 2002 to 2013, with a 3-year warm-up phase from 2002 to 2004. Subsequently, the calibrated model underwent validation from 2011 to 2022, encompassing a warm-up period of 3 years from 2011 to 2013. Table 3.7 presents the parameters, fitted values, and the corresponding minimum and maximum values obtained from 2000 simulations.

Table 3.7. Calibrated parameters for the Big Sandy Creek near Bridgeport, Texas (Sub-basin 15)

Parameters	Fitted value	Minimum value	Maximum value
V_SHALLST.gw	2278.235	1886.000	2879.000
V_DEEPST.gw	6471.060	5146.000	9326.000
V_GW_DELAY.gw	1.000	0.000	75.000
V_ALPHA_BF.gw	0.643	0.300	0.820
V_GWQMN.gw	3917.601	2925.000	4062.000
V_GW_REVAP.gw	0.141	0.100	0.160
V_REVAPMN.gw	727.763	509.000	836.000
V_RCHRG_DP.gw	0.101	0.060	0.260
V_GWHT.gw	18.451	10.900	19.650
R_CN2.mgt	-0.249	-0.270	-0.100
V_CH_N2.rte	0.044	0.000	0.090
R_CH_K2.rte	-0.305	-0.340	-0.160
V_ALPHA_BNK.rte	0.050	-0.210	0.220
R_SLSUBBSN.hru	0.133	-0.016	0.160
R_HRU_SLP.hru	0.263	0.130	0.340
R_OV_N.hru	0.167	-0.090	0.360
V_ESCO.hru	0.728	0.480	0.820
V_EPCO.hru	0.321	0.180	0.450

V__SURLAG.hru	23.195	19.000	24.000
R__CH_S1.sub	-0.258	-0.260	0.050
V__CH_K1.sub	1.07	1.00	2.10
V__CH_N1.sub	0.05	0.04	0.06

### Sub-basin 22

Sub-basin 22 serves as the primary inlet to the Eagle Mountain Lake reservoir. Calibration process for this specific sub-basin extended over an 18-year timeframe from 1990 to 2007, including a 3-year warm up from 1990 to 1992 for acclimatization. Validation process was carried out from 2005 to 2022, featuring a 3-year warm up from 2005 to 2007. Table 3.8 exhibits the parameters, their adjusted values, and the associated minimum and maximum values derived from 2,000 simulations.

Table 3.8. Calibrated parameters for the West Fork Trinity River near Boyd, Texas (Sub-basin 22)

Parameters	Fitted value	Minimum value	Maximum value
V__SHALLST.gw	4474.250	3598.000	5000.000
V__DEEPST.gw	4620.083	3464.000	6347.000
V__GW_DELAY.gw	638.950	440.000	670.000
V__ALPHA_BF.gw	0.580	0.370	0.690
V__GWQMN.gw	1685.774	628.000	1802.000
V__GW_REVAP.gw	0.152	0.140	0.180
V__REVAPMN.gw	84.995	38.000	279.000
V__RCHRG_DP.gw	0.559	0.370	0.640

V__GWHT.gw	18.130	14.000	24.000
R__CN2.mgt	-0.021	-0.080	0.120
V__CH_N2.rte	0.254	0.150	0.280
R__CH_K2.rte	0.100	0.026	0.260
V__ALPHA_BNK.rte	0.692	0.460	0.770
R__SLSUBBSN.hru	0.021	-0.100	0.100
R__HRU_SLP.hru	-0.112	-0.300	0.008
R__OV_N.hru	0.100	0.090	0.210
V__ESCO.hru	0.695	0.580	0.960
V__EPCO.hru	0.895	0.820	1.000
V__SURLAG.hru	8.232	2.800	8.500
R__CH_S1.sub	-0.034	-0.040	0.090
V__CH_K1.sub	4.477	2.370	4.600
V__CH_N1.sub	0.014	0.010	0.030

#### **Sub-basin 24**

Table 3.9 provides the parameters, fitted values, and corresponding minimum and maximum parameter values derived from 2,000 simulations conducted over 4 iterations. The calibration of sub-basin 15 (Walnut Creek at Reno, Texas) extended over a 17-year period from 1993 to 2009, including a 3-year warm-up phase from 1993 to 1995. Following calibration, the model was validated from 2007 to 2022, incorporating a warm-up period from 2007 to 2009.

Table 3.9 Calibrated parameters for the Walnut Creek at Reno, Texas (Sub-basin 24)

Parameters	Fitted_Value	Min_value	Max_value
V_SHALLST.gw	4491.414	4194.000	5000.000
V_DEEPST.gw	9688.570	7154.000	9808.000
V_GW_DELAY.gw	169.445	103.000	240.000
V_ALPHA_BF.gw	0.311	0.110	0.340
V_GWQMN.gw	3863.354	2963.000	4321.000
V_GW_REVAP.gw	0.127	0.120	0.200
V_REVAPMN.gw	842.300	587.000	863.000
V_RCHRG_DP.gw	0.159	0.000	0.180
V_GWHT.gw	3.823	1.300	7.500
R_CN2.mgt	0.006	-0.030	0.120
V_CH_N2.rte	0.173	0.079	0.180
R_CH_K2.rte	0.102	-0.100	0.120
V_ALPHA_BNK.rte	0.644	0.530	0.840
R_SLSUBBSN.hru	0.333	0.030	0.400
R_HRU_SLP.hru	-0.002	-0.310	0.040
R_OV_N.hru	-0.357	-0.370	-0.200
V_ESCO.hru	0.636	0.620	0.840
V_EPCO.hru	0.893	0.620	0.980
V_SURLAG.hru	4.941	4.700	12.000
R_CH_S1.sub	0.096	-0.020	0.230
V_CH_K1.sub	2.049	0.710	2.100
V_CH_N1.sub	0.01	0.00	0.02

## Model Performance Analysis

Five statistical measures—the coefficient of determination ( $R^2$ ), Nash-Sutcliffe efficiency (NSE), percent bias (PBIAS), Kling–Gupta efficiency (KGE) and the standard deviation of observed flow ( $\sigma_o$ ) expressed as a ratio (RSR) (Equations 2–6), were used to find the best match between the simulated and observed USGS streamflow.

The coefficient of determination, abbreviated as  $R^2$ , is a measure of how well the model replicates observed results (Touseef et al., 2020). The  $R^2$  values range from 0 to 1, with higher values indicating a better model performance and vice versa, as illustrated in Equation 2.

$$R^2 = \left[ \frac{\sum_{i=1}^n (k_i^{sim} - \bar{k}^{sim})(k_i^{obs} - \bar{k}^{obs})}{\sqrt{\sum_{i=1}^n (k_i^{sim} - \bar{k}^{sim})^2} \sqrt{\sum_{i=1}^n (k_i^{obs} - \bar{k}^{obs})^2}} \right] \quad (2)$$

Where  $obs_i$  and  $sim_i$  represent the observed and simulated data respectively.

NSE coefficient measures the efficiency of the model by relating the goodness-of-fit of the model to the variance of the measured data (Marahatta et al., 2021). The NSE values vary between negative infinity and 1, where 1 represents the best fit. NSE is computed using Equation (3):

$$NSE = 1 - \frac{\sum_{i=1}^n (k_i^{obs} - k_i^{sim})^2}{\sum_{i=1}^n (k_i^{obs} - k_i^{mean})^2} \quad (3)$$

PBIAS quantifies the average tendency of the simulated data to accurately predict the observed data (Sao et al., 2020). Positive PBIAS values indicate model underestimation and negative

values over estimation. A PBIAS value close to zero is desirable. PBIAS is, generally, expressed in percentage and is calculated using Equation (4)

$$PBIAS = \frac{\sum_{i=1}^n k_i^{sim} - k_i^{obs}}{\sum_{i=1}^n k_i^{obs}} \times 100 \quad (4)$$

The KGE was employed to simulate streamflow in comparison to corresponding observations. The KGE diagnostically dissects the NSE to offer a comprehensive measure, considering the relative significance of correlation, bias, and variability in hydrological modeling (Guzey & Önöz, 2023). KGE values span from  $-\infty$  to 1, with values closer to 1 indicating a higher level of model performance.

$$KGE = 1 - \sqrt{(r - 1)^2 - \left(\frac{\sigma_r}{\sigma_o} - 1\right)^2 - \left(\frac{\mu_r}{\mu_o} - 1\right)^2} \quad (5)$$

Where 'r' represents the Pearson product-moment correlation coefficient, while  $\sigma_s/\sigma_o$  and  $\mu_s/\mu_o$  signify the variability ratio and bias between simulations (s) and observations (o), respectively. The terms  $\sigma$  and  $\mu$  denote the standard deviation and mean of the variables, with subscripts 's' and 'o' indicating simulations and observations, respectively.

The RSR is determined by taking the ratio of the Root Mean Square Error (RMSE) to the standard deviation of the observed data, as computed by the formula 6. RSR spans from an ideal value of 0, representing perfect simulation, to larger positive values. Consequently, a lower RSR corresponds to a smaller RMSE and signifies improved simulation performance.

The calculation of RSR is carried out using Equation (6).

$$RSR = \frac{RMSE}{STDEV_{obs}} = \left[ \frac{\sqrt{\sum_{i=1}^n (Obs_i - Sim_i)}}{\sqrt{\sum_{i=1}^n (Obs_i - mean)}} \right] \quad (6)$$

## Future Climate Scenarios

### Introduction to LARS-WG

Long Ashton Research Station Weather Generator (LARS-WG) is a stochastic weather generator renowned for its capacity to simulate weather data at single sites, spanning both current and future climate scenarios (Racsco et al. (1991); Semenov et al. (1998); Semenov and Brooks (1999)). LARS-WG furnishes daily time-series data for essential climate variables, including precipitation (mm), maximum and minimum temperature (°C), and solar radiation ( $\text{MJm}^{-2}\text{day}^{-1}$ ).

LARS-WG emerged in Budapest in 1990, as part of the "Assessment of Agricultural Risk in Hungary" project, funded by the Hungarian Academy of Sciences (Racsco et al., 1991). This endeavor aimed to address the limitations of the prevailing Markov chain model concerning precipitation occurrence (Semenov et al., 1998). The conventional approach, which primarily categorizes precipitation into two states—wet or dry—based solely on the preceding day's conditions, often fails to simulate the maximum duration of dry spells accurately. This deficiency proved significant for realistic agricultural assessments, especially in regions like Hungary (Yaoming et al., 2004).

The latest iteration, LARS-WG version 8.0, underwent a comprehensive overhaul to create a robust model capable of synthesizing weather data across diverse climates. Comparative studies with another widely-used stochastic weather generator employing the Markov chain

approach (Hassan et al., 2014; Qian et al., 2005) demonstrated LARS-WG's performance to be at least on par, if not superior, across various climatic settings (Rajabi et al., 2010).

### **How LARS-WG Works**

LARS-WG has the capability to generate synthetic weather data with as little as a single year of observed weather data (Semenov et al., 2002). However, the accuracy and precision of the simulated weather data improve with a larger dataset. Using more extensive observed data enhances LARS-WG's ability to closely replicate the true climate of the specific site (Khalaf et al., 2022). It is recommended to utilize at least 20-30 years of daily weather data for optimal results. A more extended observed record, spanning several decades, is particularly advantageous for capturing less frequent climate events, such as droughts. This approach ensures that LARS-WG can effectively model and simulate these infrequent but impactful climate occurrences, contributing to a more comprehensive and accurate representation of the local climate dynamics.

The generation of weather data involves a systematic three-step process, namely site analysis, model evaluation and generator.

### **Site Analysis**

It is the initial phase of generating daily time-series weather data for a particular location identified by name, latitude and longitude. During this process, observed weather data specific to the site under consideration are thoroughly examined, leading to the creation of two distinct files: parameter file and statistics file.

The parameter file encapsulates the parameters necessary for LARS-WG to generate synthetic weather time series. It stores statistical parameters obtained from observed weather data,

serving as inputs for LARS-WG to generate synthetic weather data. The file structure initiates with the site name and location, followed by parameter details such as temperature, precipitation, and solar radiation.

Temperature modeling in LARS-WG utilizes the Fourier series, describing the annual temperature cycle using sine and cosine curves. Parameters such as mean value, amplitude, and phase angle construct these curves, with separate consideration for wet and dry days enhancing accuracy. Weather conditions on a given day are influenced by the preceding day, a concept known as autocorrelation. LARS-WG incorporates average autocorrelation values for minimum and maximum temperature and solar radiation. Solar radiation modeling relies on empirical distributions via frequency histograms, with separate modeling for wet and dry days improving representation. These parameters collectively contribute to the generation of synthetic weather data by LARS-WG, facilitating detailed simulations of weather patterns.

The statistics file includes seasonal frequency distributions for various meteorological phenomena, such as wet and dry series length and hot and cold spells. These statistical distributions are utilized in the subsequent quality test process, which involves analyzing the statistical characteristics of both observed and synthetic weather data to detect any significant differences and validate the effectiveness of the generated synthetic data.

Following the calibration of LARS-WG using observed station data, the subsequent step involves evaluating the LARS-WG's performance to assess its ability to simulate the climate at the chosen site for the intended application by using two approaches. The first method involves generating daily weather data based on information from the site parameter files. This enables offline comparisons between the observed and synthetic data. The second approach conducts a statistical comparison between synthetic weather data generated by LARS-WG and

parameters derived from observed weather data using Chi-Square goodness-of-fit, t-test, and F-test.

The Chi-squared ( $\chi^2$ ), t- and F-tests operate under the assumption that observed weather data constitute a random sample from an existing distribution, which represents the 'true' climate at the site (Sobhani et al., 2015). In this context, the null hypothesis posits that there is no difference between the 'true' climate and the simulated climate generated by LARS-WG. Conversely, the alternative hypothesis suggests that there is a difference between the two climates. The simulated climate distribution is estimated from an extended run of synthetic weather data generated by LARS-WG, utilizing parameter files obtained during the model calibration process (Goodarzi et al., 2015). These tests compare specific weather statistics derived from observed and simulated data, calculating p-values to assess the likelihood that both datasets originate from the same distribution.

A low p-value indicates that the simulated climate significantly differs from the 'true' climate. Conversely, a higher p-value suggests that the climates may be similar, although statistical tests cannot definitively prove this. Weather variables exhibiting very low p-values warrant further investigation to understand the reasons for differences. A recommended threshold for significance is a p-value less than 0.01, signaling a substantial difference between the 'true' and simulated climate for a particular variable. This suggests that, in cases where the p-value falls below 0.01, then the null hypothesis is rejected in favor of the alternative hypothesis. And, if the p-value is greater than 0.01, then the null hypothesis is not rejected.

Sample size influences the likelihood of a significant p-value. Tests are more reliable with larger datasets, providing more information about the 'true' distribution for a given climate variable. Conversely, a small sample size, indicative of limited observed data or a short-

simulated data run, offers limited insights into the true distribution for a particular climate variable.

Following the calibration of LARS-WG using observed weather data for the specific site and the subsequent verification of the weather generator's performance, synthetic weather data for the selected site is generated (Khalaf et al., 2022) mirroring the statistical characteristics of the observed weather data (Mohammadi et al., 2021). Therefore, LARS-WG, then can be employed to produce synthetic weather data aligned with a climate change scenario. This functionality allows users to simulate and study potential variations in weather patterns corresponding to different climate change scenarios, providing valuable insights into the impacts of environmental changes on the region in question.

LARS-WG can generate future temperature, precipitation, and solar radiation under different climate scenarios.

### **Creating climate scenarios from GCM output**

Global Climate Models (GCMs), also known as General Circulation Models, are complex numerical models used to simulate the Earth's climate system (Demory et al., 2020; Shiru & Chung, 2021). These models are designed to represent the interactions between the atmosphere, oceans, land surface, and ice, incorporating physical, chemical, and biological processes (Kamruzzaman et al., 2022; Tapiador et al., 2020). GCMs are crucial tools in climate science, providing insights into past climate variations, current climate conditions, and future climate projections under different scenarios. GCMs operate by dividing the Earth's atmosphere and oceans into three-dimensional grids and solving a set of mathematical equations that describe the physical processes governing atmospheric circulation, energy balance, precipitation, and other climate variables (Nguyen et al., 2022; Wang et al., 2021).

These equations are based on fundamental principles of physics, such as Newton's laws of motion and the laws of thermodynamics (Cannon, 2020; Etten-Bohm et al., 2021).

This study employed downscaled and bias-corrected precipitation and temperature projections from five GCMs available in Coupled Model Intercomparison Project Phase 6 (CMIP-6) (Das et al., 2022; Shiru & Chung, 2021). Table 3.10 provides a summary of the five GCMs integrated with LARS-WG utilized in this study, along with their respective research centers and countries of origin.

Table 3.10. GCMs from CMIP6 integrated with LARS-WG

#	Research center	Country	Global Climate Model	Grid resolution (lat, lon)
1	Commonwealth Scientific and Industrial Research Organisation (CSIRO)	Australia	ACCESS-ESM1-5	1.25° x 1.875°
2	Centre National de Recherches Meteorologiques (CNRM ), Centre Europeen de Recherche et de Formation Avancee en Calcul Scientifique ( CERFACS)	France	CNRM-CM6-1	1.40° x 1.406°
3	UK Met Office Hadley Centre (MOHC)	UK	HadGEM3-GC31-LL	1.25° x 1.88°

4	Max Planck Institute for Meteorology (MPI-M)	Germany	MPI-ESM1-2- LR	1.39° x 1.41°
5	Meteorological Research Institute (MRI)	Japan	MRI-ESM2-0	1.113° x 1.125°

CMIP-6 is a collaborative international effort that aims to improve our understanding of the Earth's climate system and to provide reliable climate projections for the future (Dike et al., 2022; Mohammadi et al., 2021). CMIP-6 builds upon previous phases of the project, with the primary goal of advancing climate modeling capabilities and addressing key scientific questions related to climate change. One of the primary objectives of CMIP-6 is to enhance the representation of Earth system processes in climate models, including improvements in simulating clouds, aerosols, land surface processes, and biogeochemical cycles (Brown et al., 2020). This allows for more accurate and comprehensive projections of future climate change and its impacts on various components of the Earth system, such as ecosystems, water resources, agriculture, and human societies. CMIP-6 involves the participation of numerous climate modeling centers from around the world, each contributing their own state-of-the-art climate models to the project (Cook et al., 2020). These models simulate the interactions between the atmosphere, oceans, land surface, and ice, incorporating physical, chemical, and biological processes (Sedlacek et al., 2023). By comparing the output from different models, scientists can assess the range of uncertainty in future climate projections and identify areas of agreement and disagreement among models.

CMIP-6 also includes the development of new experiments and scenarios to explore a wide range of possible future climate conditions. These experiments cover different greenhouse gas

emission pathways, radiative forcings, and socio-economic scenarios, allowing researchers to assess the sensitivity of the climate system to different factors and to better understand the potential impacts of future climate change (Buckton et al., 2022; Tan et al., 2021). The scenarios used in CMIP-6 are called Shared Socio-economic Pathways (SSPs), which are based on assumptions of varying levels of greenhouse gas emissions, also called radiative forcings, measured in watts per meter squared ( $\text{W}/\text{m}^2$ ) and socio-economic development trajectories by the end of the 21<sup>st</sup> century (Zhongming et al., 2022).

An overview of the five SSPs is summarized in Table 3.11. The SSPs range from a low-emissions and sustainable future (SSP1) to a high-emissions and fragmented future (SSP5). These pathways serve as plausible storylines that help researchers and policymakers explore and assess the potential impacts of climate change and society's choices (Yang et al., 2023). SSP1, known as the "Sustainability" pathway, represents a future with a strong focus on sustainable development practices and a transition to renewable energy sources. This pathway aims to limit global warming to  $1.9\text{--}2.6 \text{ W}/\text{m}^2$ . SSP2, referred to as the "Middle of the Road" scenario, represents a future where socio-economic development follows a moderate trajectory. This pathway assumes a balanced approach to economic growth, energy sources, and environmental sustainability, with a radiative forcing of  $4.5 \text{ W}/\text{m}^2$ . SSP3, labeled "Regional Rivalry," depicts a world characterized by high inequality and continued reliance on fossil fuels. This pathway envisions a future where regional conflicts and limited cooperation hinder global efforts to mitigate greenhouse gas emissions, resulting in a radiative forcing of  $7.0 \text{ W}/\text{m}^2$ . SSP4, the "Inequality" pathway, represents a future where policies are implemented to reduce greenhouse gas emissions and address social inequalities. This pathway aims to limit radiative forcing to  $6.0 \text{ W}/\text{m}^2$ . Finally, SSP5, referred to as "Fossil-driven

Development," portrays a future with high economic growth and a heavy dependence on fossil fuel resources. This pathway assumes limited climate change mitigation efforts and results in a radiative forcing of  $8.5 \text{ W/m}^2$ , representing a very high level of emissions.

Additionally, there are three distinct periods— (1) near-term period (2021–2040), (2) mid-term period (2031–2050 & 2061–2080), and (3) end-of-the-century period (2081–2100) to provide insights into how climate variables, such as precipitation and temperature may evolve and fluctuate over time at national and global scales. The near-term period focuses on the relatively immediate future and objectively assesses potential climate shifts over a shorter timeframe. It explains how precipitation, temperature, wind speed, and snow depth may change in the immediate future, i.e., the next two decades. The mid-term periods offer a medium-range outlook, providing insights into climate trends and variations over four decades. Finally, the end-of-century period represents the latter part of the century. It provides a long-term perspective on climate projections, allowing for an assessment of how precipitation, temperature, wind speed, and snow depth might change towards the later stages of this century. These projections provide valuable long-term planning and decision-making insights (O'Neill et al., 2016).

Table 3.11 Overview of CMIP6 scenarios and their corresponding SSPs

SSPs	Narrative	Radiative Forcing in 2100 (W/m <sup>2</sup> )	Explanation
SSP1	Sustainability	1.9–2.6	GHG emissions cut to net zero by 2050 and 2075
SSP2	Middle of the Road	4.5	GHG emissions will be around the current level in 2050 and then declining
SSP3	Regional Rivalry	7.0	GHG emissions double by 2100
SSP4	Inequality	6.0	GHG emissions peak by 2050 and declines
SSP5	Fossil-fueled Development	8.5	GHG emissions will double by 2050

This study made use of SSPs— SSP1-2.6, SSP2-4.5 and SSP5-8.5 with periods within the mid- and end of the century to represent mid- and long-term pathways that offer a reasonable range of possible future scenarios for the region of interest. By selecting these SSPs, this study assessed two possible future conditions and their potential impacts on regional hydrology affecting streamflow into the Eagle Mountain Lake reservoir. Research has shown that using a range of 3 to 10 GCMs in climate research and projections provides reliable and robust results (Chokkavarapu & Mandla, 2019). Therefore, this study made use of projected climatic conditions under five GCMs available in LARS-WG (Table 3.11).



## CHAPTER IV

### RESULTS

#### Model Calibration and Validation

Table 4.1. Summary of Calibration and Validation Results for Streamflow Simulation in Different Sub-basins

Sub-basin	Period	R <sup>2</sup>	NSE	KGE	RSR	PBIAS (%)
10	Calibration	0.60	0.60	0.68	0.64	3.00
	Validation	0.77	0.72	0.61	0.53	10.80
15	Calibration	0.61	0.60	0.55	0.64	-11.9
	Validation	0.74	0.61	0.48	0.62	10.6
22	Calibration	0.64	0.63	0.73	0.66	0.10
	Validation	0.72	0.72	0.80	0.53	0.10
24	Calibration	0.63	0.61	0.55	0.76	1.10
	Validation	0.62	0.62	0.71	0.62	2.20

#### Sub-basin 10

The performance metrics for both calibration and validation periods in sub-basin 10 underscore the model's reliability. Throughout both periods, the model exhibited a commendable fit, with R<sup>2</sup> values of 0.6 and 0.77, respectively, indicating strong agreements between observed and simulated streamflow. Additionally, NSE values of 0.6 and 0.72 for calibration and validation

periods underscored strong agreements between simulated and observed streamflow. Furthermore, KGE values of 0.68 and 0.61, alongside RSR values of 0.64 and 0.53 for calibration and validation, collectively suggest excellent overall model performance. Examining PBIAS values, the streamflow rate at the West Fork Trinity (sub-basin 10) was underestimated by 3.0% during calibration and 10.8% during validation. As per established criteria (Gupta et al., 2009; Moriasi et al., 2007), all indices (except PBIAS) fall within the 'very good' category, reinforcing the model's efficacy in accurately simulating streamflow in this sub-basin during both calibration and validation periods.

### **Sub-basin 15**

In sub-basin 15, the performance metrics during the calibration period were  $R^2 = 0.61$ ,  $NSE = 0.60$ ,  $KGE = 0.55$ , and  $RSR = 0.64$ . During the validation period, these metrics improved to  $R^2 = 0.74$ ,  $NSE = 0.61$ ,  $KGE = 0.48$ , and  $RSR = 0.83$ . Overall, these criteria collectively indicate strong model performance and a commendable agreement between observed and simulated streamflow. The PBIAS values during calibration (-11.9, indicating overestimation) and validation (10.6, indicating underestimation) at the same gauge site.

### **Sub-basin 22**

During both the calibration and validation periods, the  $R^2$ ,  $NSE$ ,  $KGE$ , and  $RSR$  metrics are recorded at 0.64 and 0.72, 0.61 and 0.62, 0.55 and 0.71, 0.66 and 0.62, respectively. These metrics indicate strong agreement between observed and simulated streamflow throughout both phases. Additionally, the corresponding PBIAS values of 0.1 for both calibration and validation periods indicate an underestimation in comparison to observed data across both periods.

## Sub-basin 24

The  $R^2$ , NSE, KGE, and RSR values for both calibration and validation periods stand at 0.63 and 0.62, 0.63 and 0.72, 0.73 and 0.80, 0.76 and 0.53, respectively. These values signify robust agreements between observed and simulated streamflow during both periods. The corresponding PBIAS values of 1.1 and 2.2 for calibration and validation periods indicate a slight underestimation of flow by the model in comparison to observed data during both periods.

## Historical Climate Data (1990-2022)

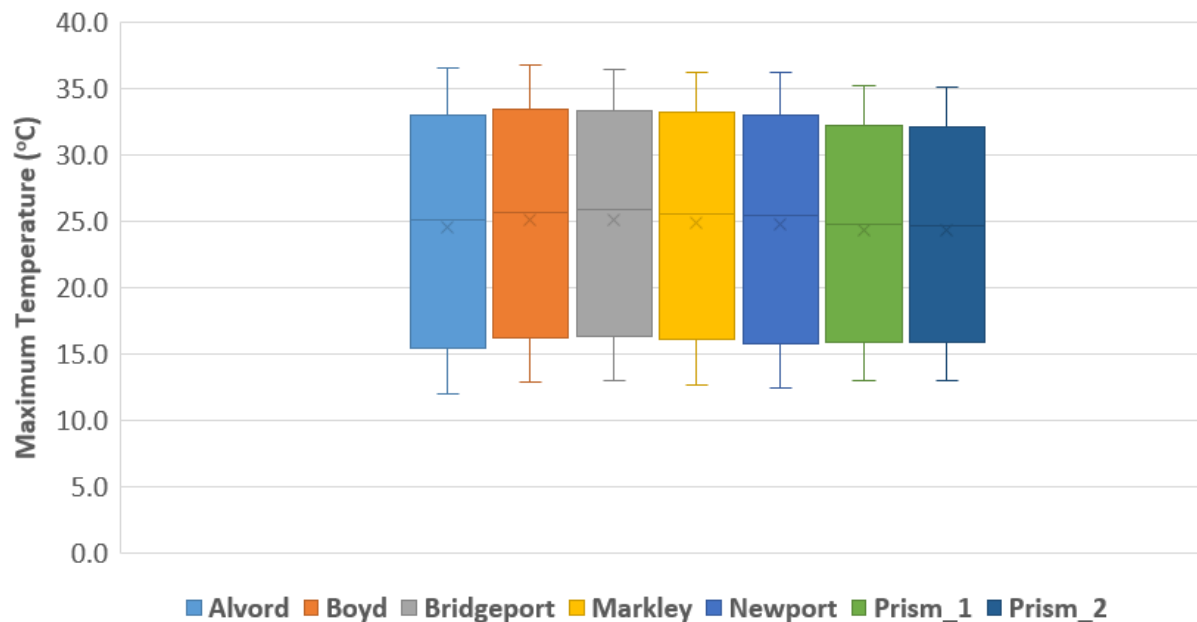


Figure 4.1. A side-by-side box plot of average monthly maximum temperature for seven stations in the watershed

In Figure 4.1, average monthly maximum temperatures are depicted through boxplots for seven distinct climate stations: Alvord, Boyd, Bridgeport, Markley, Newport, Prism\_1, and Prism\_2 for 1990 – 2022 period. The descriptive statistics for each station, including maximum (Max),

minimum (Min), first quartile (Q1), second quartile (Q2, or median), third quartile (Q3), and the overall median offer insights into the average maximum temperature distribution.

Alvord Station exhibits a maximum temperature of 36.6°C, a minimum of 12.0°C, and a median (Q2) of 24.6°C. The interquartile range (IQR), represented by the box, spans from Q1 (33.0°C) to Q3 (15.5°C), indicating the middle 50% of the data. Stations such as Alvord, Boyd, Bridgeport, Markley, and Newport consistently exhibited average monthly maximum temperatures surpassing 35°C, indicating a warmer temperature in these regions. Notably, these stations displayed relatively similar IQRs and median temperatures around 25°C, suggesting consistent warmth throughout the examined period. Conversely, Prism\_1 and Prism\_2 stations record slightly lower maximum temperatures, both below 36°C, with Prism\_2 having the lowest maximum at 35.1°C. The stations with higher maximum temperatures, including Alvord, Boyd, Bridgeport, and Markley, exhibit a broader spread, indicating increased variability in monthly maximum temperatures. The absence of skewness in the boxplots suggests a symmetrical distribution of maximum temperatures across all stations. Additionally, the lack of outliers indicates that there are no extreme values beyond the typical range observed for each station.

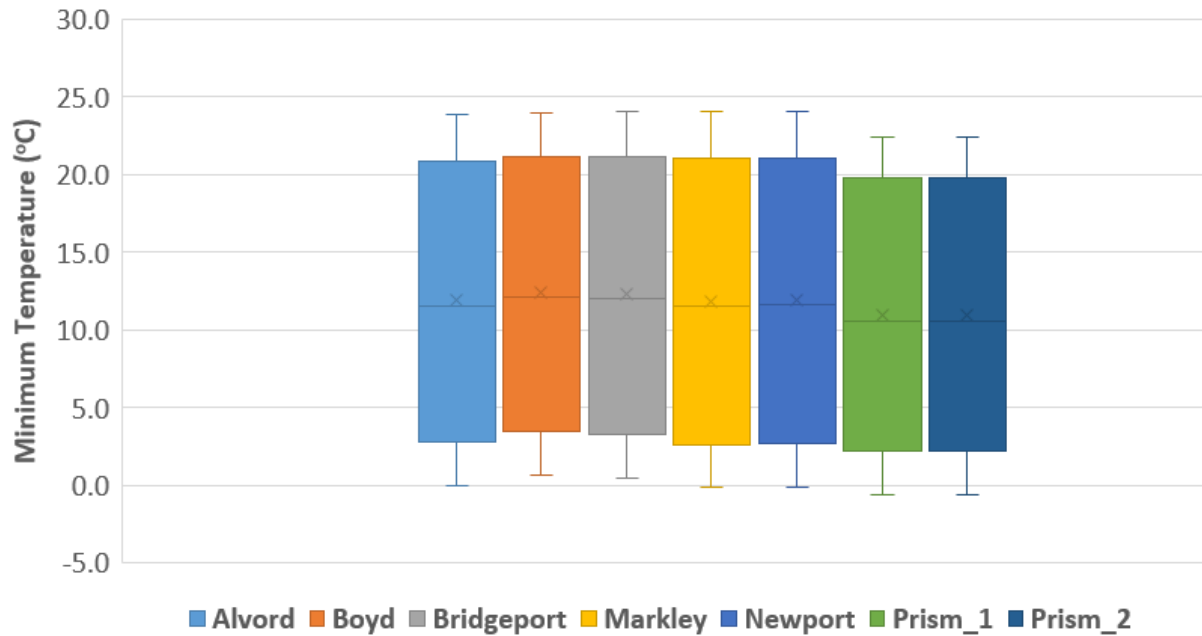


Figure 4.2. A side-by-side box plot of average monthly minimum temperature for seven stations in the watershed

The boxplot analysis of average monthly minimum temperatures across seven climate stations, including Alvord, Boyd, Bridgeport, Markley, Newport, Prism\_1, and Prism\_2 as shown in figure 4.2 offers a comprehensive understanding of the distribution characteristics of minimum temperature in the study watershed. Stations Alvord, Boyd, Markley, and Newport display a central tendency with median values clustering around 11.9°C to 12.4°C, indicative of relatively warmer minimum temperatures compared to Bridgeport, Prism\_1, and Prism\_2 stations that exhibit lower median values ranging from 10.3°C to 12.0°C, suggesting slightly cooler minimum temperatures. The IQR reveals varying degrees of spread, with Alvord, Boyd, Markley, and Newport presenting wider IQR values (18.1-17.7°C), reflecting greater variability in minimum temperatures compared to Bridgeport, Prism\_1, and Prism\_2 stations demonstrate narrower IQR values (17.6-16.9°C), indicating less variability. Notably, the

absence of outliers and skewness in the boxplot underscores a balanced distribution, assuring the reliability of the minimum temperature data.

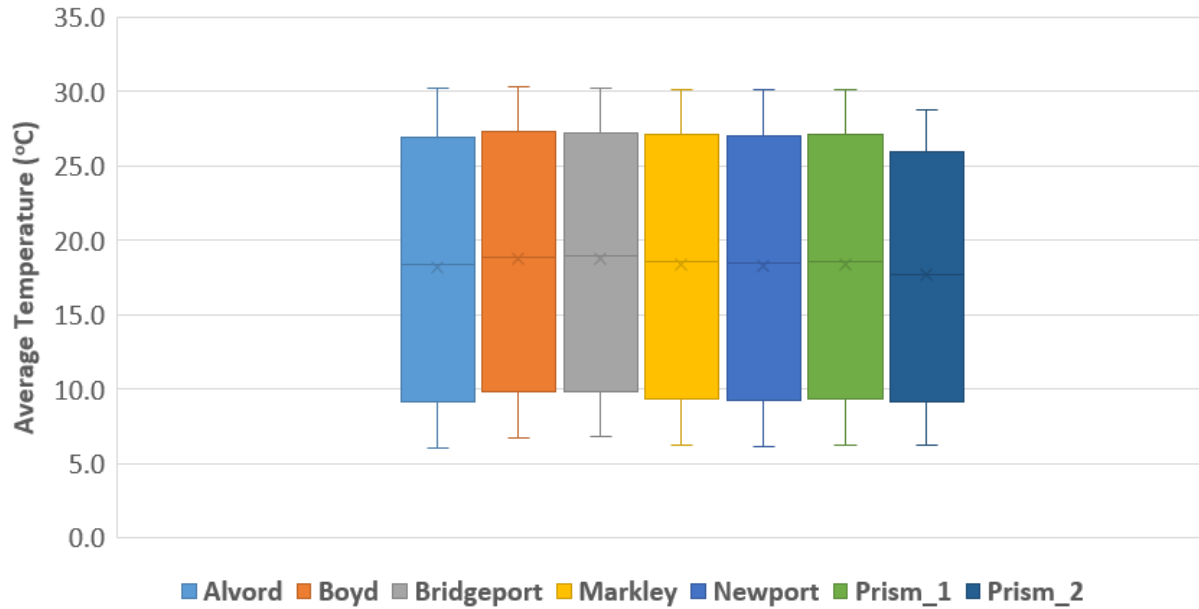


Figure 4.3. A side-by-side box plot of average monthly temperature for seven stations in the watershed

The boxplot analysis of monthly average temperatures for seven climate stations—Alvord, Boyd, Bridgeport, Markley, Newport, Prism\_1, and Prism\_2—reveals key insights into the central tendency, spread, and distribution characteristics of the data (Figure 4.3). The median average monthly temperature for each station, ranging from 17.7°C to 18.7°C, indicate the central point of the temperature distributions. Stations Boyd, Bridgeport, Markley, Newport, and Prism\_1 exhibit similar median values, suggesting comparable central tendencies in monthly average temperatures. Boyd Station has the highest median average monthly temperature (18.2°C). It suggests that, based on the given dataset, Boyd Station experiences the warmest monthly average temperatures compared to the other specified climate stations.

Conversely, Prism\_2 station displays a slightly lower median (16.5 °C), indicating a subtly cooler average temperature profile.

The IQR reflects the spread of the data, with stations Boyd, Bridgeport, Markley, Newport, and Prism\_1 showing relatively wider IQR values, indicative of greater variability in monthly average temperatures. On the other hand, Prism\_2 station demonstrates a narrower IQR, suggesting less variability. Notably, the absence of outliers and skewness in the boxplot signifies a balanced distribution of monthly average temperatures across all stations. This absence reinforces the reliability of the dataset, indicating that extreme values or asymmetry are not present, enhancing the robustness of the temperature data for further analysis.

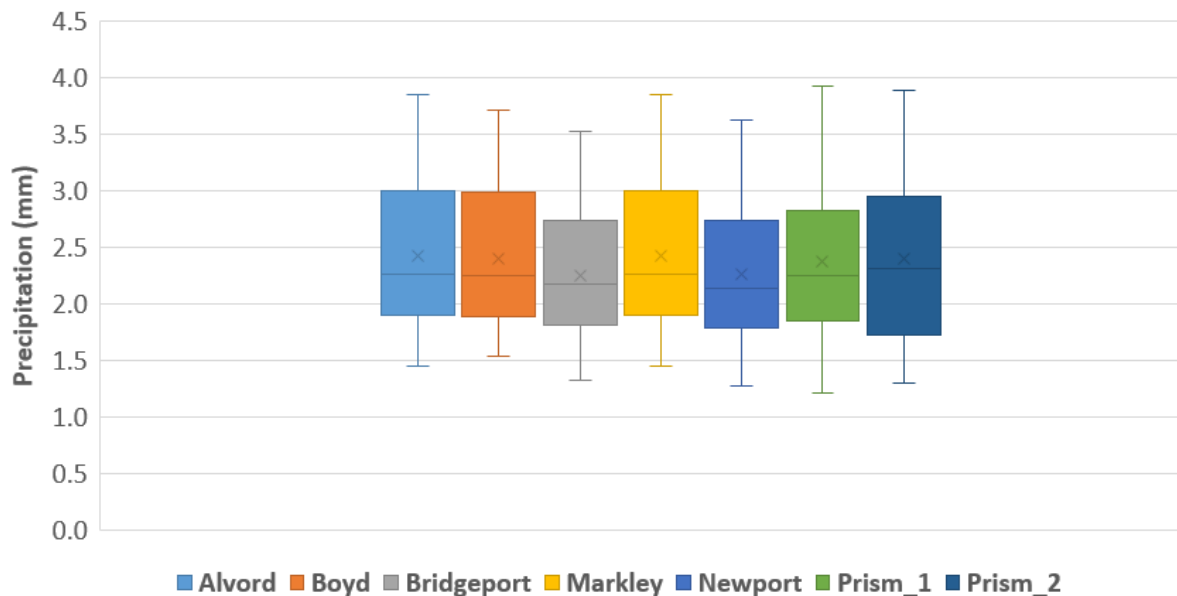


Figure 4.4. A side-by-side box plot of average monthly precipitation for seven stations in the watershed

The analysis of average precipitation data across seven climate stations—Alvord, Boyd, Bridgeport, Markley, Newport, Prism\_1, and Prism\_2—reveals consistent central tendencies

with slight variations in median precipitation levels (Figure 4.4). The median values for most stations cluster around 2.3 to 2.4 mm, indicating a relatively uniform distribution of average precipitation. Notably, Prism\_1 and Prism\_2 stations exhibit the highest mean precipitation levels, both recording a mean value of 2.5 mm. This signifies that, on average, these two stations experience slightly higher precipitation compared to the others. The interquartile range (IQR) provides insight into the spread of precipitation levels, with a moderate variability observed across the dataset (ranging from 1.8 to 2.4 mm). The dataset is identified as "Rightly Skewed," suggesting a distribution with a longer right tail. This skewness implies occasional months with higher precipitation values, contributing to the rightward extension of the distribution. Notably, the absence of outliers enhances the data's reliability for statistical analysis. Stations Prism\_1 and Prism\_2, characterized by higher maximum precipitation values and a rightward indicate occasional months with elevated precipitation levels compared to other stations. Importantly, the absence of outliers underscores the reliability of the precipitation data for statistical analysis.

### **Future vs Historical Climate Data Analysis**

Tables 4.1 and 4.2 show a comprehensive comparative analysis of future climate projections for the 2030s and 2080s, compared to the historical climate data spanning the period from 1990 to 2022, for seven climate stations (Alvord, Boyd, Bridgeport, Markley, Newport, Prism 1, and Prism 2)

Table 4.2. Comparative analysis of future temperature projections (2030s and 2080s) and historical temperature (1990-2022) for seven stations in the study watershed

Stations	GCMs	2030s (2031 – 2050) Temperature (°C)			2080s (2081 – 2100) Temperature (°C)		
		SSP1-2.6	SSP2-4.5	SSP5-8.5	SSP1-2.6	SSP2-4.5	SSP5-8.5
<b>Alvord</b>	ACCESS-ESM1-5	19.6	19.8	19.9	19.9	21.0	22.6
	CNRM-CM6-1	19.6	19.9	20.3	20.8	21.6	24.5
	HadGEM3-GC31-LL	19.2	19.4	19.8	19.5	21.3	23.8
	MPI-ESM1-2-LR	19.4	19.1	19.6	19.2	19.1	23.1
	MRI-ESM2-0	20.2	20.1	20.3	20.2	20.9	23.2
	Historical (1990-2022)	18.3					
<b>Boyd</b>	ACCESS-ESM1-5	20.2	20.4	20.4	20.4	21.5	23.2
	CNRM-CM6-1	20.1	21.3	20.8	20.4	22.1	25.0
	HadGEM3-GC31-LL	19.7	19.9	20.3	20.1	21.8	24.2
	MPI-ESM1-2-LR	19.9	19.6	20.0	19.8	21.1	23.5
	MRI-ESM2-0	20.7	20.6	20.8	20.7	21.5	23.7
	Historical (1990-2022)	18.8					
<b>Bridgeport</b>	ACCESS-ESM1-5	20.1	20.4	20.4	20.4	21.5	23.1
	CNRM-CM6-1	20.1	20.4	20.7	20.4	22.1	25.0
	HadGEM3-GC31-LL	19.7	19.9	20.3	20.0	21.8	24.2
	MPI-ESM1-2-LR	19.9	19.6	20.0	19.7	21.1	23.5

	MRI-ESM2-0	20.7	20.6	20.8	20.7	21.4	23.7
	Historical (1990-2022)	18.3					
<b>Markley</b>	ACCESS-ESM1-5	19.8	20.1	20.1	20.0	21.1	22.7
	CNRM-CM6-1	19.8	20.1	20.5	21.1	21.8	24.8
	HadGEM3-GC31-LL	19.4	19.5	20.0	19.6	21.4	23.9
	MPI-ESM1-2-LR	19.5	19.3	19.8	19.4	20.8	23.3
	MRI-ESM2-0	20.4	20.2	20.5	20.3	21.1	23.4
	Historical (1990-2022)	18.4					
<b>Newport</b>	ACCESS-ESM1-5	19.8	20.0	20.0	20.0	21.1	22.7
	CNRM-CM6-1	19.7	20.0	20.4	21.0	21.7	24.7
	HadGEM3-GC31-LL	19.3	19.5	19.9	19.6	21.4	23.9
	MPI-ESM1-2-LR	19.5	19.3	19.7	19.3	20.7	23.2
	MRI-ESM2-0	20.3	20.2	20.4	20.2	21.0	23.3
	Historical (1990-2022)	18.4					
<b>Prism 1</b>	ACCESS-ESM1-5	19.0	19.2	19.3	19.2	20.3	21.9
	CNRM-CM6-1	19.0	19.2	19.6	20.2	20.9	23.9
	HadGEM3-GC31-LL	18.6	18.7	19.1	18.8	20.6	23.1
	MPI-ESM1-2-LR	18.7	18.5	18.9	18.6	20.0	22.4
	MRI-ESM2-0	19.5	19.4	19.7	19.5	20.3	22.6
	Historical (1990-2022)	17.7					

<b>Prism 2</b>	ACCESS-ESM1-5	19.0	19.2	19.3	19.2	20.3	21.9
	CNRM-CM6-1	19.0	19.2	19.6	20.2	20.9	23.9
	HadGEM3-GC31-LL	18.6	18.7	19.1	18.8	20.6	23.1
	MPI-ESM1-2-LR	18.7	18.5	18.9	18.6	20.0	22.4
	MRI-ESM2-0	19.5	19.4	19.7	19.5	20.3	22.6
	Historical (1990-2022)	17.7					

In the Alvord station, the average temperature projections for the 2030s and 2080s under different scenarios (SSP1-2.6, SSP2-4.5, SSP5-8.5) show a consistent upward trend. For example, under the SSP1-2.6 scenario, the average temperature ranges from 19.6°C (2030s) to 22.6°C (2080s) (Table 4.1). Comparing this with the historical average temperature of 18.3°C (1990-2022), it suggests potentially hotter climatic conditions in future. Similarly, Boyd Station exhibits a rise in average temperatures for the future. In the 2030s, under the SSP5-8.5 scenario, the average temperature is projected to be 20.4°C, increasing to 23.2°C in the 2080s (Table 4.1). These projections indicate a consistent warming pattern across scenarios. Contrasting with the historical average temperature of 18.8°C (1990-2022), Boyd Station anticipates higher temperatures in the coming decades.

The Bridgeport station also shows an increasing trend in average temperatures. Under the SSP2-4.5 scenario, the average temperature is projected to rise from 19.6°C in the 2030s to 23.5°C in the 2080s (Table 4.1). This upward trajectory aligns with the warming pattern observed in the other stations. In comparison with the historical average temperature of 18.8°C (1990-2022), it indicates a potential temperature rise in the future. In the 2030s, Markley Station's projected average temperature under different scenarios (SSP1-2.6, SSP2-4.5, SSP5-8.5) ranges from 19.4°C to 20.4°C (Table 4.1). Looking ahead to the 2080s, the temperature values vary between 19.5°C and 21.4°C. Comparatively, the historical average temperature for the period 1990-2022 is 18.4°C (Table 4.1). This signifies a potential increase in temperature for the future, with the 2080s projections indicating a broader range and higher temperatures.

For Newport Station, the average temperature projections in the 2030s span from 19.3°C to 20.3°C, while the 2080s exhibit a range of 20.7°C to 21.7°C (Table 4.1). The historical average temperature from 1990-2022 is 18.4°C. Similar to Markley Station, Newport shows a trend of

increasing temperatures, with the 2080s projections indicating higher variability. Prism 1 Station anticipates average temperatures in the 2030s ranging from 18.6°C to 19.5°C (Table 4.1). In the 2080s, the projected temperatures vary from 18.8°C to 20.6°C. Historical average temperature data for 1990-2022 records an average of 17.7°C. This station, too, suggests a warming trend, with the 2080s projections indicating an elevated temperature range.

Lastly, Prism 2 Station's average temperature projections for the 2030s range from 18.5°C to 19.4°C, while the 2080s show variability between 20.0°C and 20.9°C (Table 4.1). The historical average temperature for 1990-2022 is 17.7°C (Table 4.1). Similar to the other stations, Prism 2 indicates an increasing trend in average temperatures, with the 2080s projections reflecting higher variability. Collectively, these stations demonstrate a consistent pattern of increasing average temperatures in the future, particularly in the 2080s, compared to historical averages.

Table 4.3. Comparative analysis of future precipitation projections (2030s and 2080s) and historical precipitation (1990-2022) for seven stations in the study watershed.

Stations	GCMs	2030s (2031 – 2050) Precipitation			2080s (2081 – 2100) Precipitation		
		(mm)			(mm)		
		SSP1-2.6	SSP2-4.5	SSP5-8.5	SSP1-2.6	SSP2-4.5	SSP5-8.5
<b>Alvord</b>	ACCESS-ESM1-5	2.76	2.74	2.90	2.91	2.81	2.74
	CNRM-CM6-1	3.05	3.00	2.89	2.96	3.00	2.94
	HadGEM3-GC31-LL	2.92	3.12	3.20	3.42	3.16	3.44
	MPI-ESM1-2-LR	2.59	2.66	2.57	2.53	2.66	2.13
	MRI-ESM2-0	2.51	2.75	2.79	2.49	2.89	2.64
	Historical (1990-2022)	2.43					
<b>Boyd</b>	ACCESS-ESM1-5	2.49	2.55	2.67	2.57	2.63	2.48
	CNRM-CM6-1	2.75	2.67	2.58	2.57	2.68	2.66
	HadGEM3-GC31-LL	2.66	2.81	2.97	3.07	2.86	3.02
	MPI-ESM1-2-LR	2.38	2.40	2.33	2.29	2.09	1.95
	MRI-ESM2-0	2.26	2.50	2.53	2.22	2.62	2.39
	Historical (1990-2022)	2.41					
<b>Bridgeport</b>	ACCESS-ESM1-5	2.40	2.38	2.54	2.46	2.43	2.36
	CNRM-CM6-1	2.60	2.56	2.44	2.57	2.68	2.66
	HadGEM3-GC31-LL	2.49	2.65	2.75	2.93	2.70	2.86
	MPI-ESM1-2-LR	2.21	2.24	2.19	2.13	1.94	1.78
	MRI-ESM2-0	2.12	2.33	2.36	2.08	2.47	2.29
	Historical (1990-2022)	2.26					

<b>Markley</b>	ACCESS-ESM1-5	2.56	2.47	2.67	2.67	2.52	2.55
	CNRM-CM6-1	2.82	2.70	2.64	2.66	2.72	2.66
	HadGEM3-GC31-LL	2.64	2.84	2.86	3.19	2.90	3.16
	MPI-ESM1-2-LR	2.33	2.37	2.33	2.27	2.05	1.85
	MRI-ESM2-0	2.29	2.48	2.55	2.31	2.66	2.41
	Historical (1990-2022)	2.43					
<b>Newport</b>	ACCESS-ESM1-5	2.38	2.32	2.49	2.47	2.37	2.34
	CNRM-CM6-1	2.62	2.52	2.45	2.49	2.53	2.48
	HadGEM3-GC31-LL	2.46	2.63	2.67	2.92	2.68	2.91
	MPI-ESM1-2-LR	2.18	2.23	2.16	2.13	1.93	1.76
	MRI-ESM2-0	2.13	2.31	2.34	2.11	2.45	2.26
	Historical (1990-2022)	2.26					
<b>Prism 1</b>	ACCESS-ESM1-5	2.53	2.48	2.66	2.61	2.55	2.54
	CNRM-CM6-1	2.79	2.71	2.62	2.64	2.71	2.68
	HadGEM3-GC31-LL	2.64	2.83	2.87	3.13	2.89	3.11
	MPI-ESM1-2-LR	2.33	2.38	2.31	2.27	2.04	1.86
	MRI-ESM2-0	2.25	2.47	2.52	2.26	2.62	2.41
	Historical (1990-2022)	2.37					
<b>Prism 2</b>	ACCESS-ESM1-5	2.46	2.44	2.59	2.54	2.49	2.44
	CNRM-CM6-1	2.71	2.66	2.54	2.6	2.64	2.58
	HadGEM3-GC31-LL	2.58	2.74	2.82	3.04	2.81	3.01
	MPI-ESM1-2-LR	2.29	2.33	2.27	2.22	2.00	1.86
	MRI-ESM2-0	2.20	2.39	2.44	2.18	2.55	2.34
	Historical (1990-2022)	2.40					

The projected average monthly precipitation for Alvord Station in the 2030s is expected to range from 2.51 mm to 3.20 mm/day, suggesting an increase compared to the historical period of 1990-2022, which recorded an average precipitation of 2.43 mm/day (Table 4.2). In the 2080s, the projected average monthly precipitation range is 2.49 to 3.44 mm/day, indicating a notable intensification of precipitation variability. Alvord Station is projected to experience higher levels of precipitation in the future compared to historical averages.

Markley Station shows a similar pattern, with projected precipitation in the 2030s ranging from 2.31 mm/day to 3.16 mm/day (Table 4.2). This represents a moderate increase compared to the historical period, which had an average precipitation of 2.43 mm/day (Table 4.2). For the 2080s, the range expands to 2.29 to 3.16 mm/day, suggesting an even more pronounced increase in precipitation. Markley Station anticipates elevated precipitation levels in the future compared to the historical benchmark.

In the 2030s, Boyd Station anticipates precipitation ranging from 2.18 mm/day to 3.02 mm/day, indicating a potential shift compared to the historical average of 2.41 mm (Table 4.2). The 2080s projections show a wider range from 2.05 to 3.11 mm/day, signifying increased uncertainty and variability. Historical data indicates an average precipitation of 2.41 mm/day (Table 4.2). Boyd Station is likely to experience heightened precipitation in the future compared to historical norms.

Bridgeport Station's 2030s projections range from 2.12 mm/day to 2.93 mm/day, suggesting a potential increase compared to the historical average of 2.26 mm (Table 4.2). The 2080s show a wider range from 1.78 to 3.13 mm/day, indicating increased uncertainty and variability in precipitation. Historical data records an average precipitation of 2.26 mm (Table 4.2). Bridgeport Station is expected to witness elevated precipitation levels in the future compared

to historical records. Collectively, these stations reveal a consistent trend of increased precipitation in the future, especially under the 2080s climatic conditions, compared to historical averages.

The analysis of Future Climate Projections (2030s and 2080s) and Historical Climate Data (1990-2022) for selected climate stations and GCMs is complemented by informative boxplots. These visual aids provide a comprehensive illustration of the precipitation and temperature trends across the seven stations (Alvord, Markley, Boyd, Newport, Bridgeport, Prism 1, and Prism 2) under three emission scenarios (SSP1-2.6, SSP2-4.5, and SSP5-8.5) across five GCMs.

### **Annual Streamflow**

Table 4.3 presents the average annual streamflow for the current period (2003-2022) and future periods in the 2030s and 2080s under different climate scenarios (SSP1-2.6, SSP2-4.5, and SSP5-8.5). The historical average streamflow ranges from 0.42 m<sup>3</sup>/s to 28.35 m<sup>3</sup>/s, with an overall average of 6.85 m<sup>3</sup>/s. Comparatively, under the 2030s climate, there would be a decrease in average annual streamflow for all SSP scenarios. In SSP1-2.6, the average streamflow is 5.47 m<sup>3</sup>/s, representing a decrease of 20.1% compared to the historical period. Similarly, in SSP2-4.5, the average streamflow is 5.51 m<sup>3</sup>/s, with a decrease of 19.6%, and in SSP5-8.5, it is 5.48 m<sup>3</sup>/s, with a decrease of 20.0%. Similarly, in the 2080s, the average streamflow would decrease across all SSP scenarios. In SSP1-2.6, the average streamflow is 5.58, indicating a decrease of 17.0% compared to the historical period. For SSP2-4.5, the average streamflow is 5.68 m<sup>3</sup>/s, with a decrease of 18.6%, and in SSP5-8.5, it is 5.55 m<sup>3</sup>/s, with a decrease of 18.9%. These findings highlight a general decline in streamflow projected for the future, with the magnitude of the decrease varying depending on the SSP and the time

period. Overall, the data suggests a trend of decreasing streamflow under different climate scenarios, underscoring the potential impacts of climate change on water resources. Comparison of the average streamflow for the current period with the future scenarios emphasizes the significance of these projected changes and the importance of implementing adaptive measures to address potential risks associated with declining streamflow in the future.

Table 4.4. Average annual streamflow under different climate scenarios

Average annual streamflow (m <sup>3</sup> /s) under different climatic conditions						
	2030s (2031 – 2050) Climate			2080s (2081 – 2100) Climate		
Historical	SSP 126	SSP 245	SSP 585	SSP 126	SSP 245	SSP 585
2.51	4.86	4.80	5.09	6.00	4.46	6.12
10.75	4.38	4.59	4.22	3.85	5.98	4.03
1.54	4.88	5.03	5.00	5.59	3.79	5.23
0.81	3.74	4.31	3.24	3.33	4.90	3.06
7.31	9.21	8.39	8.49	9.66	7.55	8.97
3.68	7.45	7.91	8.20	7.05	9.00	7.41
3.37	7.51	6.78	7.25	8.13	6.41	7.44
9.99	4.62	5.18	4.93	4.23	6.07	4.47
1.00	9.06	9.96	11.01	10.06	9.37	10.46
4.33	10.83	11.12	9.63	10.64	12.89	9.64
0.66	9.97	9.97	10.77	10.33	8.89	10.74
0.42	12.47	12.53	11.87	11.49	13.09	12.35
28.35	2.58	2.55	2.72	3.23	2.08	2.68

20.65	2.84	2.69	2.50	2.14	3.17	2.97
3.51	1.84	1.38	2.07	1.93	1.58	1.83
10.84	0.99	1.14	1.08	1.01	1.43	0.72
8.20	1.90	1.67	1.83	2.26	1.51	2.06
12.15	2.77	2.68	2.70	2.10	3.33	3.17
5.32	4.96	4.75	4.75	6.38	4.26	5.88
1.60	2.58	2.74	2.20	2.11	3.88	1.86

<b>Average</b>	<b>6.85</b>	<b>5.47</b>	<b>5.51</b>	<b>5.48</b>	<b>5.58</b>	<b>5.68</b>	<b>5.55</b>
----------------	-------------	-------------	-------------	-------------	-------------	-------------	-------------

<b>%</b>							
<b>Change</b>	<b>-20.1</b>	<b>-19.6</b>	<b>-20.0</b>	<b>-18.6</b>	<b>-17.0</b>	<b>-18.9</b>	

## Monthly Streamflow

Tables 4.4 and 4.5 outlines the average monthly streamflow for the historical period (2003-2022) and future periods in the 2030s and 2080s under various climate scenarios (SSP1-2.6, SSP2-4.5, and SSP5-8.5), accompanied by the percentage change in streamflow compared to the current period.

Across the historical period, average monthly streamflow exhibits considerable variability, ranging from 2.21 m<sup>3</sup>/s to 15.43 m<sup>3</sup>/s. However, under the 2030s and 2080s climatic conditions, significant changes in average monthly streamflow are evident compared to the historical period. In the 2030s, under SSP1-2.6, all twelve months experience a decrease in streamflow, with the highest decrease occurring in April (-80.4%). Under SSP2-4.5, eight out of twelve months experience a decrease, with June showing the highest reduction (-75.8%). Meanwhile, SSP5-8.5 sees a decrease in streamflow for four out of 12 months, with the highest decrease also observed in June (-41.9%). Moving to the 2080s, SSP1-2.6 shows a decrease in streamflow in eleven months, with June experiencing the highest reduction (-79.7%). SSP2-4.5 experiences a decrease in five months, with June experiencing the highest reduction (-59.5%), while SSP5-8.5 sees a decrease in four months, with the highest decrease occurring in May (-61.0%). Overall, the prevailing trend underscores a widespread decrease in streamflow for the majority of months in both the 2030s and 2080s when compared to the historical period.

While a prevalent trend of decreased streamflow is observed for most months in both the 2030s and 2080s compared to historical averages, there are instances of increased streamflow in specific months and scenarios. For example, in the 2030s, January and September show notable increases in streamflow under SSP1-2.6, with percentage increases of 48.7% and 105.0%, respectively. Moreover, under SSP5-8.5 in the 2030s, eight out of twelve months show an

increase in streamflow, with significant increases observed in August and September, reaching 252.1% and 125.3%, respectively. Similarly, in the 2080s, under SSP2-4.5, seven months exhibit an increase in streamflow, with noteworthy increases of 111.2% and 146.5% in August and September, respectively. Additionally, under SSP5-8.5, eight months show an increase in streamflow, with notable increases of 126.5% and 131.7% observed in July and August, respectively. This pattern highlights the potential implications of climate change on streamflow dynamics, underscoring the necessity for adaptive strategies to mitigate potential risks associated with evolving water resources.

Table 4.5. Average monthly streamflow under different climate scenarios in the study watershed

Average monthly streamflow (m <sup>3</sup> /s) under							
Historical		2030s (2031 – 2050)			2080s (2081 -2100)		
Month	Historical	SSP 126	SSP 245	SSP 585	SSP 126	SSP 245	SSP 585
Jan	5.13	3.16	7.62	8.49	3.60	8.33	4.37
Feb	6.05	3.03	4.15	10.00	3.12	6.85	7.63
Mar	8.73	3.23	5.32	7.28	2.67	6.09	9.22
Apr	7.75	2.29	3.81	10.18	3.06	6.16	6.90
May	10.21	3.26	6.77	7.48	3.49	7.70	3.98
Jun	15.43	3.02	3.73	8.96	3.14	6.24	7.26
Jul	3.91	3.46	4.64	6.25	2.65	5.07	8.85
Aug	2.72	2.21	3.48	9.58	3.18	5.75	6.30
Sep	3.81	3.33	7.80	8.57	3.77	9.38	4.26
Oct	5.86	2.97	4.45	9.41	3.34	7.52	7.23
Nov	7.67	3.27	5.17	7.26	2.86	5.87	9.11
Dec	5.26	2.40	3.86	10.12	2.64	5.75	6.61

Table 4.6. Percentage (%) change in future monthly streamflow compared to the historical climate

Change (%) in streamflow compared to historical
---

Month	2030s (2031 – 2050)			2080s (2081 – 2100)		
	SSP 126	SSP 245	SSP 585	SSP 126	SSP 245	SSP 585
Jan	<b>-38.3</b>	48.7	65.7	<b>-29.8</b>	62.5	<b>-14.7</b>
Feb	<b>-50.0</b>	<b>-31.5</b>	65.2	<b>-48.4</b>	13.2	26.0
Mar	<b>-63.0</b>	<b>-39.0</b>	<b>-16.6</b>	<b>-69.4</b>	<b>-30.2</b>	5.6
Apr	<b>-70.4</b>	<b>-50.9</b>	31.3	<b>-60.5</b>	<b>-20.5</b>	<b>-11.0</b>
May	<b>-68.1</b>	<b>-33.7</b>	<b>-26.7</b>	<b>-65.8</b>	<b>-24.6</b>	<b>-61.0</b>
Jun	<b>-80.4</b>	<b>-75.8</b>	<b>-41.9</b>	<b>-79.7</b>	<b>-59.5</b>	<b>-53.0</b>
Jul	<b>-11.5</b>	18.9	59.9	<b>-32.2</b>	29.9	126.5
Aug	<b>-18.6</b>	27.9	252.1	16.8	111.2	131.7
Sep	<b>-12.5</b>	105.0	125.3	<b>-1.0</b>	146.5	12.0
Oct	<b>-49.2</b>	<b>-24.0</b>	60.7	<b>-43.0</b>	28.4	23.4
Nov	<b>-57.3</b>	<b>-32.6</b>	<b>-5.4</b>	<b>-62.7</b>	<b>-23.5</b>	18.7
Dec	<b>-54.3</b>	<b>-26.7</b>	92.3	<b>-49.8</b>	9.2	25.6
# of months with decrease in streamflow	12.0	8.0	4.0	11.0	5.0	4.0
% months with decreased streamflow	100	67	33	92	42	33

Note: Bold indicates months with decreased streamflow.



## CHAPTER V

### DISCUSSION

Several studies have reported the impact of climate change on the hydrology of various types of watersheds all over the world, from predominantly agricultural watersheds, to watersheds in the arid regions, including data-scarce watersheds (Candela et al., 2012; Daneshvar et al., 2021; Dennedy-Frank & Gorelick, 2019; Eshete et al., 2022; Samimi et al., 2020; Touseef et al., 2020). Similarly, in this study the SWAT-based model of the Upper West Fork Trinity Watershed was developed to understand the potential effects of climate change on the watershed streamflow that support one of the major reservoirs in the DFW region. This study is the first to examine climate impact on water resources in this watershed at the local watershed scale.

#### **Model Performance**

In this study, a SWAT model for the historical period 1990-2022 for Upper West Fork Trinity Watershed was successfully developed. A graphical comparison of the observed streamflow derived from the developed SWAT model shows that generally the model-simulated data are consistent with trends in the observed data. To confirm the model performance, a statistical evaluation of the simulated versus the observed data was then performed. The calibrated, validated model was considered to have strong agreement with the observed streamflow data. Statistical evaluation of the model performance was done using five objective functions in SWAT-CUP: PBIAS,  $R^2$ , NSE, KGE, and RSR. For the purpose of the study focus, the USGS gaging station located in sub-basin 22 was selected as it is drained by the majority of the watershed and serves as the main streamflow inlet to Eagle Mountain Lake.

PBIAS quantifies the average tendency of the simulated data to accurately predict the observed data in terms of under- or over-prediction of the model output compared to the observation (Sao et al., 2020). Positive PBIAS values indicate model overestimation, and negative values underestimation. The PBIAS values for the calibration and the validation PBIAS values of 0.1% for both calibration and validation periods indicate a virtually unbiased model in comparison to observed streamflow across both periods.  $R^2$  measures the proportion of variance in observed data compared to the model, i.e., it tracks the model's accuracy in tracking variations in the observed data. The possible value of  $R^2$  ranges from 0 to 1, with values closer to one indicating low error variance. An acceptable  $R^2$  value is a value  $>0.5$  (Touseef et al., 2020). For this study  $R^2$  values were 0.64 and 0.72 for the calibration and validation periods, respectively, indicating that the model was able to explain 64 to 72% of the variability in the streamflow.

NSE measures the goodness of fit between the simulated data and observed data. NSE values range from negative infinity ( $-\infty$ ) to 1.0, and as the value approaches one, the simulation better represents the observation robustly. The NSE values are 0.63 and 0.72 for the calibrated and validated time periods, respectively, indicating an adequate fit with the observed streamflow. KGE values span from  $-\infty$  to 1, with values closer to 1 indicating a higher level of model performance (Guzey & Önöz, 2023). The RSR is determined by taking the ratio of the Root Mean Square Error (RMSE) to the standard deviation of observed (actual) data, as computed by the following formula. RSR spans from an ideal value of 0, representing perfect simulation, to larger positive values. KGE, and RSR metrics are recorded at 0.66 and 0.62, respectively. These metrics indicate good agreement between observed and simulated streamflow during model calibration and validation periods.

The statistical values derived for this SWAT model are comparable to those of other SWAT studies. For example, Sharma (2023) had  $R^2$  and NSE values of 0.60 and 0.59, respectively, for a climate sensitivity analysis for watersheds in the Rio Grande basin of New Mexico. Muche et al. (2020) reported a KGE value of 0.61 and an RSR value of 0.64 for a SWAT model in a Kansas agricultural watershed to study climate change impacts on streamflow. Chen et al. (2021) determined that  $R^2 = 0.7$  and  $NSE = 0.79$  for a SWAT model of a watershed in the Upper Mississippi River to study climate change impacts on runoff predictions. In these previous SWAT studies, climate change analyses were performed after the researchers found acceptable objective function values. Therefore, the objective function values derived in this SWAT model for the Upper West Fork Trinity Watershed were considered satisfactory to perform a climate change analysis.

### **Impacts of Climate Change in the Study Watershed**

Climate change analysis was performed with the calibrated model parameters in ArcSWAT and then used to create hydrographs of the future scenario of SSP1-2.6, SSP2-4.5, SSP5-8.5 under the 2030s (2031 – 2050), 2080s (2081 – 2100), and the historical (2003 – 2022) climatic conditions for the monthly average streamflow. Across all seven stations in the study watershed, there is a consistent trend of increasing average temperatures in both the 2030s and 2080s under all three SSPs compared to historical averages. For instance, in Alvord Station, the average temperature is projected to increase by approximately 3°C from 19.6°C in the 2030s to 22.6°C in the 2080s under the SSP5-8.5 scenario, indicating a hotter climate than the historical.

Comparing the temperature increases observed in the Upper West Fork Trinity Watershed with findings from other studies conducted in watersheds across the US and around the world

reveals consistent warming trends. Studies in various US watersheds have reported increasing temperatures due to climate change, with projections aligning with the trends observed in the Upper West Fork Trinity Watershed. For instance, research in the Sierra Nevada Mountains projects temperature increases of approximately 3.5°C by the end of the century under high emissions scenarios (Beltran-Peña, 2023). Similarly, studies in the Colorado River Basin anticipate temperature increases of 1.5°C to 2.5°C by mid-century, with even greater warming by the end of the century under SSP5-8.5 (Hancock, 2020). Internationally, studies in watersheds such as the Amazon Basin and the Rhine River Basin also project significant temperature increases by the end of the century, further corroborating the warming trends observed in the Upper West Fork Trinity Watershed. For example, projections for the Amazon Basin suggest temperature increases of approximately 4.3°C by the end of the century (Costa et al., 2023), while the Rhine River Basin anticipates temperature increases of 2.0°C to 3.7°C by the end of the century (Hundhausen et al., 2022).

The projected average annual precipitation for our study watershed is expected to increase by up to 28% in the 2030s and by up to 32% in the 2080s compared to the 2003 – 2022 precipitation, with a few months showing decrease by up to 33% and increase by up to 116% across three SSPs. However, in various watersheds across the US, studies have shown trends of increasing and decreasing precipitation under future climate scenarios. For example, research conducted in watersheds in the Pacific Northwest, such as the Columbia River Basin, has indicated a projected increase in precipitation due to climate change, ranging from approximately 5% to 20% under different emission scenarios (Queen et al., 2021). Similarly, studies in the Northeastern US, including watersheds like the Delaware River Basin, have also suggested an uptick in precipitation in the future, with percentage increases ranging from

approximately 3% to 15% under various emission scenarios (Woltemade et al., 2020). Meanwhile, in the Central America and the Caribbean region, projections paint a different picture, indicating potential decreases in precipitation under different emissions scenarios. For SSP1-2.6, there is a projected precipitation decrease of 2% to 5% by 2080. Under SSP2-4.5, this decrease becomes more pronounced, ranging from 5% to 10% by 2080 (Almazroui et al., 2021). The highest emissions scenario, SSP5-8.5, predicts the most significant decrease in precipitation, with projections ranging from 10% to 15% by 2080.

According to the 2015 National Climate Assessment (Van Den Besselaar et al., 2015), projections indicate a rise in precipitation of 10-20% by the end of the century (2070-2099) in the US. Similarly, temperature projections for the same period suggest an estimated increase of approximately 1.3°C to 3.7°C under lower emissions scenarios and 3.0°C to 6.1°C under higher emissions scenarios. In examining the specific conditions within our watershed, the projections reveal similar trends. Our watershed is anticipated to experience a substantial temperature rise, ranging from 1.0°C to 5.0°C average annual temperature, with some months showing an average increase of as high as 6.2°C. These temperature projections are comparable to those estimated by the NCA, indicating a potentially warming trend. These projected precipitation and temperature ranges signify increased uncertainty and variability in future climatic conditions in the study watershed. These findings underscore the urgent need for proactive measures to mitigate and adapt to the impacts of climate change in our watershed.

### **Impacts of Climate Change on Streamflow**

The analysis of projected climate change impacts on streamflow dynamics within the Upper West Fork Trinity Watershed provides valuable insights into future water resource dynamics. Overall, the analysis indicates a projected decrease in streamflow in the future compared to the

2003 – 2022 historical record. Under both the 2030s and 2080s climate, the model predicts an increase in both average annual temperature and precipitation across all scenarios relative to current periods. However, when looking at the monthly scale, precipitation projections suggest a decrease during summer and an increase during fall and winter seasons. These shifts in temperature and precipitation patterns are reflected in the projected streamflow in the watershed. Regardless of SSPs, the average annual streamflow in the watershed is projected to decrease by 17 to 20% under future climatic conditions compared to the 2003 – 2022 observed streamflow. Lower streamflow during spring and early summer months are anticipated, with occasional exceptions showing increased flow in July through October. For example, SSP 585 under the 2030s climate project streamflow could increase by more than two-fold in August (2.72 m<sup>3</sup>/s historical vs. 9.58 m<sup>3</sup>/s). Some of these fluctuations in streamflow appear disproportionate to changes in precipitation and temperature. These disparities may stem from various factors, including differences in precipitation and temperature intensity, soil saturation levels, or alterations in other hydrological components such as evapotranspiration, snowmelt, groundwater flow, baseflow, and land use patterns in the watershed.

In analyzing the streamflow results, it becomes evident that the projected changes have significant implications for water availability in the lake, particularly when considering seasonal variations. The anticipated decrease in streamflow during spring months (March, April and May) by approximately 38% on average under both the 2030s and 2080s climate could potentially reduce water levels in the Eagle Mountain Lake reservoir. However, the projected increase in average streamflow of 18% over the summer months (June, July, and August), a 12% increase over the fall months (September, October, and November), and 3.6% increase in winter months (December, January and February) could potentially could

potentially offset the spring water level deficiency in the reservoir. However, the increase in streamflow in summer, fall, and winter could result in riverine and lake flooding. However, the summer and fall months typically coincide with the warmer seasons, where water demand may be higher for various purposes such as irrigation, recreation, and municipal use. Therefore, the projected increase in streamflow during these months could potentially benefit the region.

The significant 252% increase in streamflow during August under the SSP 585 scenario in the 2030s, which is often considered a high-emission or "worst-case" pathway, suggests a drastic deviation from historical norms that could be driven by a combination of factors. This includes more intense and frequent rain events as predicted by climate models due to global warming, which could lead to sudden surges in streamflow during this month. If preceding months are particularly wet, the soil may reach saturation, leading to increased runoff into river systems. Changes in land use, such as deforestation or urbanization, exacerbate these effects by reducing the land's ability to absorb rainfall.

The notable increases in streamflow under certain scenarios, such as those projected for Eagle Mountain Lake, bring numerous benefits, including an enhanced water supply for agriculture, increased hydroelectric power generation, and improved river health, which supports biodiversity (Kiedrzyńska et al., 2021; Siddha & Sahu, 2022). However, these benefits are accompanied by challenges, especially when Eagle Mountain Lake, the primary water storage system in this study, reaches its full capacity (Morway et al., 2023; Shao et al., 2023). Balancing the benefits and risks associated with increased streamflow becomes crucial.

When Eagle Mountain Lake is at full capacity, any additional influx from increased streamflow can lead to flooding (Liu et al., 2024). This presents significant risks to infrastructure, homes, and agricultural lands around the lake, potentially causing extensive damage and disrupting

local communities (Merz et al., 2021; Mishra et al., 2022). Managing these situations requires precise operational decisions to safely release water while maintaining the structural integrity of the lake's dam and other water control structures. Moreover, while increased streamflow can enhance the lake's ecosystem, excessive flow can erode lake shores, destroy habitats, and alter aquatic environments, negatively impacting species that rely on stable conditions (Siddha & Sahu, 2022).

To effectively manage these dynamics at Eagle Mountain Lake, adaptive management strategies are essential. This includes enhancing the lake's infrastructure to handle higher volumes of water, thus preventing overflow and facilitating controlled releases during peak flows. Implementing Integrated Water Resource Management (IWRM) can help coordinate the multiple uses and users of water resources around the lake, ensuring sustainability (Tariq et al., 2021). Furthermore, developing comprehensive flood management plans that include early warning systems and community evacuation plans can mitigate the risks associated with sudden increases in water levels (Kotecha et al., 2024). Continuous environmental monitoring and conservation efforts are also crucial in preserving the ecological balance of Eagle Mountain Lake and mitigating the adverse impacts of changes in water flow. These combined strategies ensure that the benefits of increased streamflow are realized without compromising the safety and environmental integrity of the Eagle Mountain Lake area (Ganoulis, 2023).

Despite some cases where streamflow increases, the overall trend indicates a future with less water available, particularly impacting domestic and industrial water supply and recreational activities (Siirila-Woodburn et al., 2021). This reduction in streamflow could lead to consistently lower water levels in Eagle Mountain Lake, affecting the volume of water available for household and industrial uses. Industries relying on a consistent water supply

might face operational challenges and increased costs, potentially impacting the broader economy (Rodrigues et al., 2023). Recreational activities around Eagle Mountain Lake, such as fishing, boating, and other water sports, would likely be adversely affected. Lower water levels can restrict access to parts of the lake, complicating boat navigation and diminishing the overall quality of the recreational experience (Chalise et al., 2021; Rodrigues et al., 2023). This could result in a decline in tourism, negatively affecting businesses dependent on visitors, such as local shops, restaurants, and hotels (Ngin et al., 2020).

The ecological health of the lake and its surroundings could also suffer as habitats reliant on certain water levels are altered or reduced (Cantonati et al., 2020). This scenario could lead to decreased biodiversity and affect various species that are integral to the aquatic and surrounding ecosystems (Adeogun & Chukwuka, 2023). Given these potential impacts, proactive planning and management strategies are crucial. Community leaders and local authorities might need to implement more stringent water conservation measures, invest in infrastructure to better manage water resources, and develop programs to support local economy and ecological conservation efforts. Effective management of the lake's water resources will be essential to sustaining the community and the natural environment in light of these projected changes in streamflow.

Our results align with findings from various previous studies that have explored similar watersheds or regions, providing valuable insights into potential variations in streamflow dynamics. These studies have collectively contributed to our understanding of how streamflow may respond to climate change scenarios. For instance, a study conducted by Paul (2023) in the Nooksack River watershed in northwestern Washington projected a decrease in streamflow of approximately 15% in the summer months (June-August) by the 2080s under a high

emissions scenario. Similarly, Quansah et al. (2021) examined streamflow changes in the Alabama River Basin and reported a decrease of 10% in August streamflow by the 2030s under a moderate emissions scenario. Furthermore, Miller et al. (2021) analyzed streamflow projections in a broader regional context in the southwestern region of the United States and found significant decreases in streamflow across multiple months by the 2080s under high emissions scenarios. While their study focused on a larger geographical area, our results corroborate their findings. Quantitatively, when comparing the percentage changes in streamflow across specific months and scenarios, our study shows similar trends to those reported in these previous studies. However, the magnitude of changes may vary due to differences in watershed characteristics, climate models, emission scenarios, and modeling techniques employed.

However, it is essential to note that these fluctuations in streamflow reflect the dynamic interplay between climate factors, hydrological processes, and water availability. Changes in precipitation patterns, temperature regimes, and other environmental variables can significantly influence streamflow dynamics and, consequently, water availability in the lake. Therefore, understanding these complex relationships and adapting management strategies accordingly is crucial for effectively navigating the potential impacts of climate change on water resources.

### **Model Limitations**

Hydrological models, such as SWAT, aim to simulate complex natural environments, yet they often encounter challenges due to data availability and model limitations. In our study, the use of SWAT was hindered by the unavailability of crucial climate data, particularly relative humidity, wind speed, and solar radiation. As a result, we used a simple form of

evapotranspiration method (Hargreaves). Furthermore, it is important to note that our study focused on annual and monthly streamflow estimates. This limitation may restrict our ability to capture short-term variations (daily and sub-daily) in streamflow patterns, potentially overlooking important temporal dynamics within the watershed. Consequently, it could introduce uncertainties, particularly when analyzing events such as flash floods or rapid changes in streamflow. Relying only on annual and monthly averages may mask extreme events or fluctuations that could have significant implications for water resource management and decision-making. Therefore, while our study provides valuable insights into long-term trends and general patterns, it may not fully capture the complete spectrum of streamflow dynamics at finer temporal scales.

Another limitation of our methodology was the reliance on a single land cover dataset, specifically from the year 2016. Hydrological models are sensitive to changes in land cover, as these changes can significantly affect water runoff, evaporation, and overall watershed dynamics. Using only one year's data does not account for subsequent changes in land use and land cover that can occur over time due to factors like urbanization, deforestation, or agricultural expansion. Ideally, using different land cover datasets for different years would provide a more accurate reflection of the watershed's changing conditions and how these changes impact water resources.

It is essential to acknowledge these limitations when interpreting the results of our study, particularly when considering management changes within the watershed. However, despite these challenges, our study successfully achieved its primary objective of examining the impact of climate-induced precipitation and temperature changes on water resources, with a specific focus on streamflow. By shedding light on these critical aspects, our study contributes valuable

insights into the potential effects of climate change on water resource dynamics, facilitating informed decision-making and adaptive management strategies in the face of evolving environmental conditions.

## **Recommendation**

In light of the identified limitations in our study, several recommendations can be made to improve future research and enhance the robustness of hydrological modeling in similar watersheds. First and foremost, efforts should be directed towards enhancing data collection and availability. Comprehensive datasets encompassing various hydrological parameters, including additional climate variables such as relative humidity, wind speed, and solar radiation, should be collected and implemented in the model. This will improve the accuracy and reliability of hydrological models, enabling better representation of complex watershed evapotranspiration processes.

Moreover, hydrological models should aim to strike a balance between complexity and computational efficiency. While physically-based models like SWAT offer detailed representations of hydrological processes, efforts should be made to continually refine and validate these models against observed data at different temporal and spatial resolutions to ensure they accurately capture the dynamics of the watershed. Integrating uncertainty analysis techniques into hydrological modeling frameworks can provide valuable insights into the reliability and robustness of model outputs. By quantifying uncertainty associated with input data, model parameters, and structural assumptions, researchers can enhance the credibility of model predictions and improve decision-making under uncertainty.

Collaboration between hydrologists, climatologists, geographers, and other relevant disciplines can foster interdisciplinary research approaches, enriching hydrological modeling

efforts and leading to more comprehensive assessments of climate change impacts on water resources. Establishing long-term monitoring programs to continuously collect data on hydrological processes within the watershed is essential. Regular evaluation of model performance against observed data can help identify areas for improvement and refine model structures and parameterizations over time. Lastly, engaging stakeholders, including local communities, policymakers, and water resource managers, is crucial for ensuring that research findings are effectively communicated and translated into actionable strategies. By fostering dialogue and collaboration with stakeholders, researchers can ensure that hydrological modeling efforts address relevant societal needs and contribute to sustainable water resource management in similar watersheds.

## **CHAPTER VI**

### **Conclusion**

The Upper West Fork Trinity Watershed was studied using SWAT to assess the effects of climate change on streamflow. The study aimed to quantify how changes in climate patterns would influence the watershed hydrology, specifically streamflow. To achieve this, the SWAT model was calibrated and validated against observed streamflow data from six USGS gauging stations. The calibration and validation results demonstrated reasonable accuracy in monthly streamflow projections, effectively capturing a substantial portion of observed streamflow variability. Utilizing downscaled and bias-corrected precipitation and temperature projections from LARS-WG GCMs for the 2030s and 2080s climatic conditions, ArcSWAT was employed to analyze the watershed's climate change impact. This rigorous approach instilled confidence in the results, revealing the potential for increased average temperature, rainfall, and decreased streamflow in the Upper West Fork Trinity Watershed. Overall, the study findings suggest that SWAT-based model of the watershed is able to represent the watershed hydrology well and provided useful insights on potential future changes in the streamflow dynamics.

## References

- Abbass, K., Qasim, M. Z., Song, H., Murshed, M., Mahmood, H., & Younis, I. (2022). A review of the global climate change impacts, adaptation, and sustainable mitigation measures. *Environmental Science and Pollution Research*, 29(28), 42539-42559.
- Abbaspour, K. C., Rouholahnejad, E., Vaghefi, S., Srinivasan, R., Yang, H., & Kløve, B. (2015). A continental-scale hydrology and water quality model for Europe: Calibration and uncertainty of a high-resolution large-scale SWAT model. *Journal of Hydrology*, 524, 733-752.
- Abbass, K., Qasim, M. Z., Song, H., Murshed, M., Mahmood, H., & Younis, I. (2022). A review of the global climate change impacts, adaptation, and sustainable mitigation measures. *Environmental Science and Pollution Research*, 29(28), 42539-42559.
- Adeogun, A. O., & Chukwuka, A. V. (2023). Anthropogenic impacts as determinants of tropical lake morphology: Inferences for strategic conservation of lake wetland biodiversity.
- Almazroui, M., Islam, M. N., Saeed, F., Saeed, S., Ismail, M., Ehsan, M. A., Diallo, I., O'Brien, E., Ashfaq, M., & Martínez-Castro, D. (2021). Projected changes in temperature and precipitation over the United States, Central America, and the Caribbean in CMIP6 GCMs. *Earth Systems and Environment*, 5, 1-24.
- Arnold, J. G., Srinivasan, R., Muttiah, R. S., & Williams, J. R. (1998). Large area hydrologic modeling and assessment part I: model development 1. *JAWRA Journal of the American Water Resources Association*, 34(1), 73-89.
- AWWA. (2020). *American Water Works Association-State of Water Industry* [https://doi.org/https://www.awwa.org/Portals/0/Awwa/ETS/Resources/SOTWI\\_2021\\_Full\\_Report.pdf](https://doi.org/https://www.awwa.org/Portals/0/Awwa/ETS/Resources/SOTWI_2021_Full_Report.pdf)
- Badora, D., Wawer, R., Nierobca, A., Krol-Badziak, A., Kozyra, J., Jurga, B., & Nowocien, E. (2022). Modelling the hydrology of an upland catchment of Bystra River in 2050 climate using RCP 4.5 and RCP 8.5 emission scenario forecasts. *Agriculture*, 12(3), 403.
- Bariamis, G., & Baltas, E. (2021). Hydrological Modeling in Agricultural Intensive Watershed: The Case of Upper East Fork White River, USA. *Hydrology*, 8(3), 137.
- Beltran-Peña, A. A. (2023). *Evaluating Climate Change Impacts on Water Resources and Food Systems—A Global Perspective With Insights From Africa and California*. University of California, Berkeley.
- Ben Saad, A., Ben M'barek-Jemai, M., Ben M'barek, N., & Mezza, S. (2023). Hydrological modeling of the watershed of a RAMSAR site using the SWAT model (Ichkeul National Park—Tunisia of the extreme north). *Modeling Earth Systems and Environment*, 9(2), 2783-2795.
- Borchardt, S., & Choi, W. (2023). Effects of climate change and high-capacity wells pumping on streamflow and groundwater elevation in Northeastern Wisconsin. *Environmental Earth Sciences*, 82(6), 148.

- Brown, J. R., Brierley, C. M., An, S.-I., Guarino, M.-V., Stevenson, S., Williams, C. J., Zhang, Q., Zhao, A., Abe-Ouchi, A., & Braconnot, P. (2020). Comparison of past and future simulations of ENSO in CMIP5/PMIP3 and CMIP6/PMIP4 models. *Climate of the Past*, 16(5), 1777-1805.
- Brown, T. C., Mahat, V., & Ramirez, J. A. (2019). Adaptation to future water shortages in the United States caused by population growth and climate change. *Earth's Future*, 7(3), 219-234.
- Bucton, B. G. B., Shrestha, S., Saurav, K., Mohanasundaram, S., Viridis, S. G., & Chaowiwat, W. (2022). Impacts of climate and land use change on groundwater recharge under shared socioeconomic pathways: A case of Siem Reap, Cambodia. *Environmental Research*, 211, 113070.
- Candela, L., Tamoh, K., Olivares, G., & Gomez, M. (2012). Modelling impacts of climate change on water resources in ungauged and data-scarce watersheds. Application to the Siurana catchment (NE Spain). *Science of The Total Environment*, 440, 253-260.
- Cannon, A. J. (2020). Reductions in daily continental-scale atmospheric circulation biases between generations of global climate models: CMIP5 to CMIP6. *Environmental Research Letters*, 15(6), 064006.
- Cantonati, M., Poikane, S., Pringle, C. M., Stevens, L. E., Turak, E., Heino, J., Richardson, J. S., Bolpagni, R., Borrini, A., & Cid, N. (2020). Characteristics, main impacts, and stewardship of natural and artificial freshwater environments: consequences for biodiversity conservation. *Water*, 12(1), 260.
- CBF. (2020). *Carbon brief-* <https://www.carbonbrief.org/mapped-how-climate-change-affects-extreme-weather-around-the-world/>
- Chalise, D. R., Sankarasubramanian, A., & Ruhi, A. (2021). Dams and climate interact to alter river flow regimes across the United States. *Earth's Future*, 9(4), e2020EF001816.
- Chauhan, M., Phillips, C., Rooth, J., Whiteway, M., Wineland, B., & Portugal, J. (2020). *Water Policy and Sustainability (Tarrant County, Texas)*.
- Chen, M., Cui, Y., Gassman, P. W., & Srinivasan, R. (2021). Effect of watershed delineation and climate datasets density on runoff predictions for the Upper Mississippi River Basin using SWAT within HAWQS. *Water*, 13(4), 422.
- Chokkavarapu, N., & Mandla, V. R. (2019). Comparative study of GCMs, RCMs, downscaling and hydrological models: a review toward future climate change impact estimation. *SN Applied Sciences*, 1(12), 1698.
- Cole, H. D., Cole, M. J., Simpson, K. J., Simpson, N. P., Ziervogel, G., & New, M. G. (2021). Managing city-scale slow-onset disasters: Learning from Cape Town's 2015–2018 drought disaster planning. *International Journal of Disaster Risk Reduction*, 63, 102459.
- Cook, B. I., Mankin, J. S., Marvel, K., Williams, A. P., Smerdon, J. E., & Anchukaitis, K. J. (2020). Twenty-first century drought projections in the CMIP6 forcing scenarios. *Earth's Future*, 8(6), e2019EF001461.
- Costa, A. A., Guimarães, S. O., Sales, D. C., das Chagas Vasconcelos Junior, F., Marinho, M. W. S., Pereira, J. M. R., Martins, E. S. P. R., & da Silva, E. M. (2023). Precipitation extremes over the tropical Americas under RCP4. 5 and RCP8. 5 climate change scenarios:

- Results from dynamical downscaling simulations. *International Journal of Climatology*, 43(2), 787-803.
- Daneshvar, F., Frankenberger, J. R., Bowling, L. C., Cherkauer, K. A., & Moraes, A. G. d. L. (2021). Development of strategy for SWAT hydrologic modeling in data-scarce regions of Peru. *Journal of Hydrologic Engineering*, 26(7), 05021016.
- Das, S., Kamruzzaman, M., Islam, A. R. M. T., Zhu, D., & Kumar, A. (2022). Comparison of Future Changes in Frequency of Climate Extremes between Coastal and Inland Locations of Bengal Delta Based on CMIP6 Climate Models. *Atmosphere*, 13(11), 1747.
- de Oliveira Serrão, E. A., Silva, M. T., Ferreira, T. R., de Ataíde, L. C. P., dos Santos, C. A., de Lima, A. M. M., da Silva, V. d. P. R., de Sousa, F. d. A. S., & Gomes, D. J. C. (2022). Impacts of land use and land cover changes on hydrological processes and sediment yield determined using the SWAT model. *International Journal of Sediment Research*, 37(1), 54-69.
- Demory, M.-E., Berthou, S., Fernández, J., Sørland, S. L., Brogli, R., Roberts, M. J., Beyerle, U., Seddon, J., Haarsma, R., & Schär, C. (2020). European daily precipitation according to EURO-CORDEX regional climate models (RCMs) and high-resolution global climate models (GCMs) from the High-Resolution Model Intercomparison Project (HighResMIP). *Geoscientific Model Development*, 13(11), 5485-5506.
- Dennedy-Frank, P. J., & Gorelick, S. M. (2019). Insights from watershed simulations around the world: Watershed service-based restoration does not significantly enhance streamflow. *Global environmental change*, 58, 101938.
- Dike, V. N., Lin, Z., Fei, K., Langendijk, G. S., & Nath, D. (2022). Evaluation and multimodel projection of seasonal precipitation extremes over central Asia based on CMIP6 simulations. *International Journal of Climatology*, 42(14), 7228-7251.
- Eagle-Mountain-Revenue. (2022). <https://www.zippia.com/eagle-mountain-careers-449635/revenue/>
- Edamo, M. L., Bushira, K. M., Ukumo, T. Y., Ayele, M. A., Alaro, M. A., & Borko, H. B. (2022). Effect of climate change on water availability in Bilate catchment, Southern Ethiopia. *Water Cycle*, 3, 86-99.
- Ercan, M. B., Maghami, I., Bowes, B. D., Morsy, M. M., & Goodall, J. L. (2020). Estimating potential climate change effects on the upper neuse watershed water balance using the SWAT model. *JAWRA Journal of the American Water Resources Association*, 56(1), 53-67.
- Erler, A. R., Frey, S. K., Khader, O., d'Orgeville, M., Park, Y. J., Hwang, H. T., Lapen, D. R., Richard Peltier, W., & Sudicky, E. A. (2019). Simulating climate change impacts on surface water resources within a lake-affected region using regional climate projections. *Water Resources Research*, 55(1), 130-155.
- Eshete, D. G., Rigler, G., Shinshaw, B. G., Belete, A. M., & Bayeh, B. A. (2022). Evaluation of streamflow response to climate change in the data-scarce region, Ethiopia. *Sustainable Water Resources Management*, 8(6), 187.
- Etten-Bohm, M., Yang, J., Schumacher, C., & Jun, M. (2021). Evaluating the relationship between lightning and the large-scale environment and its use for lightning prediction in global climate models. *Journal of Geophysical Research: Atmospheres*, 126(5), e2020JD033990.

- Galan, D., Smith, T., & Yoder, J. (2020). Supporting Local Health Departments and Partners to Prepare for and Respond to Water Emergencies. *Journal of Public Health Management and Practice*, 26(1), 91-93.
- Ganoulis, J. (2023). A New Dialectical Model of Water Security under Climate Change. *Water*, 15(14), 2672.
- Getirana, A., Libonati, R., & Cataldi, M. (2021). Brazil is in water crisis—it needs a drought plan. *Nature*, 600(7888), 218-220.
- Goodarzi, E., Dastorani, M., & Talebi, A. (2015). Evaluation of the Change-factor and LARS-WG methods of downscaling for simulation of climatic variables in the future (Case study: Herat Azam Watershed, Yazd-Iran). *Ecopersia*, 3(1), 833-846.
- Guerra, J. F., & Debbage, N. (2021). Changes in urban land use throughout the Edwards Aquifer: A comparative analysis of Austin, San Antonio, and the Interstate–35 corridor. *Applied Geography*, 133, 102480.
- Gupta, H. V., Kling, H., Yilmaz, K. K., & Martinez, G. F. (2009). Decomposition of the mean squared error and NSE performance criteria: Implications for improving hydrological modelling. *Journal of Hydrology*, 377(1-2), 80-91.
- Guzey, G. E., & Önöz, B. (2023). Performance Assessment Comparison between Physically Based and Regression Hydrological Modelling: Case Study of the Euphrates–Tigris Basin. *Sustainability*, 15(13), 10657.
- Hancock, C. L. (2020). *Spatial and Temporal Controls on Streamflow Variability in the San Juan Mountains, Colorado* [University of Denver].
- Hassan, Z., Shamsudin, S., & Harun, S. (2014). Application of SDSM and LARS-WG for simulating and downscaling of rainfall and temperature. *Theoretical and Applied Climatology*, 116, 243-257.
- Hines, E., & Reid, C. E. (2020). Hurricane Harvey hospital flood impacts: Accuracy of federal emergency management agency flood hazard areas in Harris County, Texas. *American journal of public health*, 110(4), 574-579.
- Hoegh-Guldberg, O., Jacob, D., Taylor, M., Guillén Bolaños, T., Bindi, M., Brown, S., Camilloni, I. A., Diedhiou, A., Djalante, R., & Ebi, K. (2019). The human imperative of stabilizing global climate change at 1.5 C. *Science*, 365(6459), eaaw6974.
- Hosseini, S. H., & Khaleghi, M. R. (2020). Application of SWAT model and SWAT-CUP software in simulation and analysis of sediment uncertainty in arid and semi-arid watersheds (case study: The Zoshk–Abardeh watershed). *Modeling Earth Systems and Environment*, 6(4), 2003-2013.
- Hundhausen, M., Feldmann, H., Laube, N., & Pinto, J. G. (2022). Future heat extremes and impacts in a convection permitting climate ensemble over Germany. *Natural Hazards and Earth System Sciences Discussions*, 2022, 1-29.
- IPCC. (2014a). Climate change 2014: impacts, adaptation, and vulnerability. Part A: global and sectoral aspects. Contribution of Working Group II to the fifth assessment report of the Intergovernmental Panel on Climate Change. *Cambridge University Press, Cambridge, United Kingdom and New York, NY, USA*.
- IPCC. (2014b). <https://reliefweb.int/report/world/climate-change-food-security-and-small-scale-producers-analysis-findings>

[fifth?gclid=Cj0KCQjw8qmhBhCIARIsANAtboc2EMaE90HzInQcmiL1PJvhlcZc zo9V55DwbPmpogA9QEEAHH5dwkaAhFfeALw wcb.](#)

- Kamruzzaman, M., Shahid, S., Roy, D. K., Islam, A. R. M. T., Hwang, S., Cho, J., Zaman, M. A. U., Sultana, T., Rashid, T., & Akter, F. (2022). Assessment of CMIP6 global climate models in reconstructing rainfall climatology of Bangladesh. *International Journal of Climatology*, 42(7), 3928-3953.
- Kang, X., Qi, J., Li, S., & Meng, F.-R. (2022). A watershed-scale assessment of climate change impacts on crop yields in Atlantic Canada. *Agricultural Water Management*, 269, 107680.
- Khalaf, R. M., Hussein, H., Hassan, W. H., Mohammed, Z. M., & Nile, B. K. (2022). Projections of precipitation and temperature in Southern Iraq using a LARS-WG Stochastic weather generator. *Physics and Chemistry of the Earth, Parts A/B/C*, 128, 103224.
- Khalid, K., Ali, M. F., Abd Rahman, N. F., Mispan, M. R., Haron, S. H., Othman, Z., & Bachok, M. F. (2016). Sensitivity analysis in watershed model using SUFI-2 algorithm. *Procedia engineering*, 162, 441-447.
- Khan, I., Lei, H., Shah, A. A., Khan, I., & Muhammad, I. (2021). Climate change impact assessment, flood management, and mitigation strategies in Pakistan for sustainable future. *Environmental Science and Pollution Research*, 28, 29720-29731.
- Kiedrzyńska, E., Belka, K., Jarosiewicz, P., Kiedrzyński, M., & Zalewski, M. (2021). The enhancement of valley water retentiveness in climate change conditions. *Science of The Total Environment*, 799, 149427.
- Kim, J.-T., Lee, C.-H., & Lee, N. (2022). Improvement and Analysis for Accuracy of Baseflow Using SWAT-CUP Premium in the Yongjeon Stream, South Korea.
- Kotecha, M. J., Bakori, D., Agarwal, S., Meraj, G., Kanga, S., Singh, S. K., & Farooq, M. (2024). Geoinformation for integrated urban water resource management. In *Earth Observation in Urban Monitoring* (pp. 93-111). Elsevier.
- Kreienkamp, F., Philip, S. Y., Tradowsky, J. S., Kew, S. F., Lorenz, P., Arrighi, J., Belleflamme, A., Bettmann, T., Caluwaerts, S., & Chan, S. C. (2021). Rapid attribution of heavy rainfall events leading to the severe flooding in Western Europe during July 2021. *World Weather Attribution*.
- Leigh, N. G., & Lee, H. (2019). Sustainable and resilient urban water systems: The role of decentralization and planning. *Sustainability*, 11(3), 918.
- Li, C., & Fang, H. (2021). Assessment of climate change impacts on the streamflow for the Mun River in the Mekong Basin, Southeast Asia: using SWAT model. *Catena*, 201, 105199.
- Little, M. (2005). *Camper's Guide to Texas Parks, Lakes, and Forests: Where to Go and how to Get There*. Taylor Trade Publishing.
- Liu, Y., Liu, F., Chen, C., Chen, Q., Zhang, J., Mo, K., Jiang, Q., & Yao, S. (2024). A holistic approach to projecting streamflow and analyzing changes in ecologically relevant hydrological indicators under climate and land use/cover change. *Journal of Hydrology*, 130863.
- Loáiciga, H. A., & Schofield, M. (2019). Climate variability, climate change, and Edwards Aquifer water fluxes.

- Los-Angeles-Times. (2022). *'Full-on crisis': Groundwater in California's Central Valley disappearing at alarming rate.*
- Mace, R. E. (2019). The use of water from the Edwards Aquifers, Texas.
- Makarigakis, A. K., & Jimenez-Cisneros, B. E. (2019). UNESCO's contribution to face global water challenges. *Water, 11*(2), 388.
- Malik, M. A., Dar, A. Q., & Jain, M. K. (2022). Modelling streamflow using the SWAT model and multi-site calibration utilizing SUFI-2 of SWAT-CUP model for high altitude catchments, NW Himalaya's. *Modeling Earth Systems and Environment, 1*-11.
- Manandhar, B., Cui, S., Wang, L., & Shrestha, S. (2023). Post-Flood Resilience Assessment of July 2021 Flood in Western Germany and Henan, China. *Land, 12*(3), 625.
- Marahatta, S., Devkota, L. P., & Aryal, D. (2021). Application of SWAT in hydrological simulation of complex Mountainous river basin (part I: model development). *Water, 13*(11), 1546.
- Mariappan, S., David Raj, A., Kumar, S., & Chatterjee, U. (2023). Global Warming Impacts on the Environment in the Last Century. In *Ecological Footprints of Climate Change: Adaptive Approaches and Sustainability* (pp. 63-93). Springer.
- Marsooli, R., Lin, N., Emanuel, K., & Feng, K. (2019). Climate change exacerbates hurricane flood hazards along US Atlantic and Gulf Coasts in spatially varying patterns. *Nature Communications, 10*(1), 3785.
- Mbow, H.-O. P., Reisinger, A., Canadell, J., & O'Brien, P. (2017). Special Report on climate change, desertification, land degradation, sustainable land management, food security, and greenhouse gas fluxes in terrestrial ecosystems (SR2). *Ginevra, IPCC, 650*.
- McManamay, R. A., DeRolph, C. R., Surendran-Nair, S., & Allen-Dumas, M. (2019). Spatially explicit land-energy-water future scenarios for cities: Guiding infrastructure transitions for urban sustainability. *Renewable and Sustainable Energy Reviews, 112*, 880-900.
- Melosi, M. V. (2021). 6 DALLAS-FORT: WORTH MARKETING THE METROPLEX. In *Sunbelt cities* (pp. 162-195). University of Texas Press.
- Merz, B., Blöschl, G., Vorogushyn, S., Dottori, F., Aerts, J. C., Bates, P., Bertola, M., Kemter, M., Kreibich, H., & Lall, U. (2021). Causes, impacts and patterns of disastrous river floods. *Nature Reviews Earth & Environment, 2*(9), 592-609.
- Miller, O. L., Putman, A. L., Alder, J., Miller, M., Jones, D. K., & Wise, D. R. (2021). Changing climate drives future streamflow declines and challenges in meeting water demand across the southwestern United States. *Journal of Hydrology X, 11*, 100074.
- Mishra, A., Mukherjee, S., Merz, B., Singh, V. P., Wright, D. B., Villarini, G., Paul, S., Kumar, D. N., Khedun, C. P., & Niyogi, D. (2022). An overview of flood concepts, challenges, and future directions. *Journal of Hydrologic Engineering, 27*(6), 03122001.
- Mohammadi, H., Khalili, R., & Mohammadi, S. (2021). Forecasting future temperature and precipitation under the effects of climate change using the LARS-WG climate generator (Case Study: South Zagros Region of Iran. *Nivar, 45*(114-115), 137-153.
- Moriasi, D. N., Arnold, J. G., Van Liew, M. W., Bingner, R. L., Harmel, R. D., & Veith, T. L. (2007). Model evaluation guidelines for systematic quantification of accuracy in watershed simulations. *Transactions of the ASABE, 50*(3), 885-900.

- Morway, E. D., Buto, S. G., Niswonger, R. G., & Huntington, J. L. (2023). *Assessing potential effects of changes in water use in the middle Carson River Basin with a numerical groundwater-flow model, Eagle, Dayton, and Churchill Valleys, west-central Nevada* (2328-0328).
- Muche, M. E., Sinnathamby, S., Parmar, R., Knightes, C. D., Johnston, J. M., Wolfe, K., Purucker, S. T., Cyterski, M. J., & Smith, D. (2020). Comparison and evaluation of gridded precipitation datasets in a Kansas agricultural watershed using SWAT. *JAWRA Journal of the American Water Resources Association*, 56(3), 486-506.
- Naresh, R., Jat, P., Chandra, M. S., Gupta, S., Gawdiya, S., Shivangi, B. K. P., Chandel, S., & Pandey, B. (2021). Water-saving technologies and modeling of withdrawal, allocation and consumptive use of surface water and groundwater resources in RWCS: A review. *Pharma Innovation Journal*, 10, 118-131.
- Naz, B. S., Kao, S.-C., Ashfaq, M., Gao, H., Rastogi, D., & Gangrade, S. (2018). Effects of climate change on streamflow extremes and implications for reservoir inflow in the United States. *Journal of Hydrology*, 556, 359-370.
- NCA. (2018). *NCA4 Volume II: Impacts, Risks, and Adaptation in the United States (2018)* <https://www.globalchange.gov/nca4>
- Neitsch, S. L., Arnold, J. G., Kiniry, J. R., & Williams, J. R. (2011). *Soil and water assessment tool theoretical documentation version 2009*.
- Ngin, C., Chhom, C., & Neef, A. (2020). Climate change impacts and disaster resilience among micro businesses in the tourism and hospitality sector: The case of Kratie, Cambodia. *Environmental Research*, 186, 109557.
- Nguyen, P. L., Bador, M., Alexander, L. V., Lane, T. P., & Ngo-Duc, T. (2022). More intense daily precipitation in CORDEX-SEA regional climate models than their forcing global climate models over Southeast Asia. *International Journal of Climatology*, 42(12), 6537-6561.
- Nielsen-Gammon, J. W., Banner, J. L., Cook, B. I., Tremaine, D. M., Wong, C. I., Mace, R. E., Gao, H., Yang, Z. L., Gonzalez, M. F., & Hoffpauir, R. (2020). Unprecedented drought challenges for Texas water resources in a changing climate: what do researchers and stakeholders need to know? *Earth's Future*, 8(8), e2020EF001552.
- NOAA. (2020). . n.d.-a. "Climate Change and Extreme Snow in the US." n.d.-a. <https://www.ncdc.noaa.gov/news/climate-change-and-extreme-snow-us>.
- Noor, M., Ismail, T., Shahid, S., Asaduzzaman, M., & Dewan, A. (2022). Projection of rainfall intensity-duration-frequency curves at ungauged location under climate change scenarios. *Sustainable Cities and Society*, 83, 103951.
- Nyatuame, M., Amekudzi, L. K., & Agodzo, S. K. (2020). Assessing the land use/land cover and climate change impact on water balance on Tordzie watershed. *Remote Sensing Applications: Society and Environment*, 20, 100381.
- Pal, S., Wang, J., Feinstein, J., Yan, E., & Kotamarthi, V. R. (2023). Projected changes in extreme streamflow and inland flooding in the mid-21st century over Northeastern United States using ensemble WRF-Hydro simulations. *Journal of Hydrology: Regional Studies*, 47, 101371.

- Paul, E. A. (2023). Modeling 21st Century Peak Flows in the Nooksack River Basin in Northwestern Washington State Using Dynamically-Downscaled Global Climate Model Projections.
- Pee, L. G., & Pan, S. L. (2022). Climate-intelligent cities and resilient urbanisation: Challenges and opportunities for information research. *International Journal of Information Management*, 63, 102446.
- Perez-Quesada, G., Hendricks, N. P., & Steward, D. R. (2020). Quantifying the economic costs of High Plains Aquifer depletion.
- Peters-Lidard, C. D., Rose, K. C., Kiang, J. E., Strobel, M. L., Anderson, M. L., Byrd, A. R., Kolian, M. J., Brekke, L. D., & Arndt, D. S. (2021). Indicators of climate change impacts on the water cycle and water management. *Climatic Change*, 165, 1-23.
- Pokhrel, Y., Felfelani, F., Satoh, Y., Boulange, J., Burek, P., Gädeke, A., Gerten, D., Gosling, S. N., Grillakis, M., & Gudmundsson, L. (2021). Global terrestrial water storage and drought severity under climate change. *Nature Climate Change*, 11(3), 226-233.
- Qian, B., Hayhoe, H., & Gameda, S. (2005). Evaluation of the stochastic weather generators LARS-WG and AAFC-WG for climate change impact studies. *Climate research*, 29(1), 3-21.
- Quansah, J. E., Naliaka, A. B., Fall, S., Ankumah, R., & Afandi, G. E. (2021). Assessing future impacts of climate change on streamflow within the Alabama River basin. *Climate*, 9(4), 55.
- Queen, L. E., Mote, P. W., Rupp, D. E., Chegwidan, O., & Nijssen, B. (2021). Ubiquitous increases in flood magnitude in the Columbia River basin under climate change. *Hydrology and Earth System Sciences*, 25(1), 257-272.
- Racsko, P., Szeidl, L., & Semenov, M. (1991). A serial approach to local stochastic weather models. *Ecological Modelling*, 57(1-2), 27-41.
- Rajabi, A., Sedghi, H., Eslamian, S., & Musavi, H. (2010). Comparison of Lars-WG and SDSM downscaling models in Kermanshah (Iran). *Ecol Environ Conserv*, 16(4), 1-7.
- Rodrigues, D., Fonseca, A., Stolarski, O., Freitas, T. R., Guimarães, N., Santos, J. A., & Fraga, H. (2023). Climate change impacts on the Côa Basin (Portugal) and potential impacts on agricultural irrigation. *Water*, 15(15), 2739.
- Rossetto, R., De Filippis, G., Triana, F., Ghetta, M., Borsi, I., & Schmid, W. (2019). Software tools for management of conjunctive use of surface-and ground-water in the rural environment: integration of the Farm Process and the Crop Growth Module in the FREEWAT platform. *Agricultural Water Management*, 223, 105717.
- Roy, P. S., Ramachandran, R. M., Paul, O., Thakur, P. K., Ravan, S., Behera, M. D., Sarangi, C., & Kanawade, V. P. (2022). Anthropogenic land use and land cover changes—A review on its environmental consequences and climate change. *Journal of the Indian Society of Remote Sensing*, 50(8), 1615-1640.
- Saade, J., Atieh, M., Ghanimeh, S., & Golmohammadi, G. (2021). Modeling impact of climate change on surface water availability using SWAT model in a semi-arid basin: case of El Kalb River, Lebanon. *Hydrology*, 8(3), 134.
- Samimi, M., Mirchi, A., Moriasi, D., Ahn, S., Alian, S., Taghvaeian, S., & Sheng, Z. (2020). Modeling arid/semi-arid irrigated agricultural watersheds with SWAT: Applications, challenges, and solution strategies. *Journal of Hydrology*, 590, 125418.

- Sao, D., Kato, T., Tu, L. H., Thouk, P., Fitriyah, A., & Oeurng, C. (2020). Evaluation of different objective functions used in the sufi-2 calibration process of swat-cup on water balance analysis: A case study of the Pursat river basin, Cambodia. *Water*, *12*(10), 2901.
- Sedlacek, J., Sukhodolov, T., Egorova, T., Karagodin-Doyennel, A., & Rozanov, E. (2023). Future climate under CMIP6 solar activity scenarios. *Earth and Space Science*, *10*(7), e2022EA002783.
- Semenov, M. A., Barrow, E. M., & Lars-Wg, A. (2002). A stochastic weather generator for use in climate impact studies. *User Man Herts UK*, 1-27.
- Semenov, M. A., & Brooks, R. J. (1999). Spatial interpolation of the LARS-WG stochastic weather generator in Great Britain. *Climate research*, *11*(2), 137-148.
- Semenov, M. A., Brooks, R. J., Barrow, E. M., & Richardson, C. W. (1998). Comparison of the WGEN and LARS-WG stochastic weather generators for diverse climates. *Climate research*, *10*(2), 95-107.
- Shao, M., Fernando, N., Zhu, J., Zhao, G., Kao, S. C., Zhao, B., Roberts, E., & Gao, H. (2023). Estimating Future Surface Water Availability Through an Integrated Climate-Hydrology-Management Modeling Framework at a Basin Scale Under CMIP6 Scenarios. *Water Resources Research*, *59*(7), e2022WR034099.
- Sharma, A. P. M., Jhahharia, D., Gupta, S., & Yurembam, G. S. (2022). Multiple indices based agricultural drought assessment in Tripura, northeast India. *Arabian Journal of Geosciences*, *15*(7), 636.
- Sharma, S. (2023). *Hydrological Modeling Using Different Precipitation Datasets for Watersheds in the Rio Grande Basin of New Mexico, USA* [New Mexico State University].
- Sharp Jr, J. M., Green, R. T., & Schindel, G. M. (2019). *The Edwards aquifer: the past, present, and future of a vital water resource* (Vol. 215). Geological Society of America.
- Shiru, M. S., & Chung, E.-S. (2021). Performance evaluation of CMIP6 global climate models for selecting models for climate projection over Nigeria. *Theoretical and Applied Climatology*, *146*(1-2), 599-615.
- Siddha, S., & Sahu, P. (2022). Impact of climate change on the river ecosystem. In *Ecological significance of river ecosystems* (pp. 79-104). Elsevier.
- Siirila-Woodburn, E. R., Rhoades, A. M., Hatchett, B. J., Huning, L. S., Szinai, J., Tague, C., Nico, P. S., Feldman, D. R., Jones, A. D., & Collins, W. D. (2021). A low-to-no snow future and its impacts on water resources in the western United States. *Nature Reviews Earth & Environment*, *2*(11), 800-819.
- Singh, V., Bankar, N., Salunkhe, S. S., Bera, A. K., & Sharma, J. (2013). Hydrological stream flow modelling on Tungabhadra catchment: parameterization and uncertainty analysis using SWAT CUP. *Current science*, 1187-1199.
- Singson, C. L., Alejo, L. A., Balderama, O. F., & Bareng, J. L. F. (2023). Modeling climate change impact on the inflow of the Magat reservoir using the Soil and Water Assessment Tool (SWAT) model for dam management. *Journal of Water and Climate Change*.
- Sobhani, B., Eslahi, M., & Babaeian, I. (2015). Efficiency of statistical downscaling models of SDSM and LARS-WG in the simulation of meteorological parameters in Lake Urmia basin. *Physical geography research quarterly*, *47*(4), 499-516.

- Sunde, M. G., He, H. S., Hubbart, J. A., & Urban, M. A. (2017). Integrating downscaled CMIP5 data with a physically based hydrologic model to estimate potential climate change impacts on streamflow processes in a mixed-use watershed. *Hydrological Processes*, 31(9), 1790-1803.
- Swain, D., Wing, O. E., Bates, P. D., Done, J., Johnson, K., & Cameron, D. (2020). Increased flood exposure due to climate change and population growth in the United States. *Earth's Future*, 8(11), e2020EF001778.
- Swain, S., Mishra, S., Pandey, A., Pandey, A., Jain, A., Chauhan, S., & Badoni, A. K. (2022). Hydrological modelling through SWAT over a Himalayan catchment using high-resolution geospatial inputs. *Environmental Challenges*, 8, 100579.
- Talukder, B., Ganguli, N., Matthew, R., Hipel, K. W., & Orbinski, J. (2022). Climate change-accelerated ocean biodiversity loss & associated planetary health impacts. *The Journal of Climate Change and Health*, 100114.
- Tan, M. L., Liang, J., Samat, N., Chan, N. W., Haywood, J. M., & Hodges, K. (2021). Hydrological extremes and responses to climate change in the kelantan river basin, malaysia, based on the CMIP6 highresmpip experiments. *Water*, 13(11), 1472.
- Tapiador, F. J., Navarro, A., Moreno, R., Sánchez, J. L., & García-Ortega, E. (2020). Regional climate models: 30 years of dynamical downscaling. *Atmospheric Research*, 235, 104785.
- Tariq, M. A. U. R., Wangchuk, K., & Muttill, N. (2021). A critical review of water resources and their management in Bhutan. *Hydrology*, 8(1), 31.
- Tefera, G. W., & Ray, R. L. (2023). Hydrology and hydrological extremes under climate change scenarios in the Bosque watershed, North-Central, Texas, USA.
- Texas-Climate-Summaries. (2022). *ASSESSMENT of HISTORIC and FUTURE TRENDS of EXTREME WEATHER IN TEXAS, 1900-2023*
- Texastribune. (2023). *Texas tribune* <https://www.texastribune.org/2023/04/03/texas-senate-bill-28-water-supply/>.
- Touseef, M., Chen, L., Masud, T., Khan, A., Yang, K., Shahzad, A., Wajid Ijaz, M., & Wang, Y. (2020). Assessment of the future climate change projections on streamflow hydrology and water availability over Upper Xijiang River Basin, China. *Applied Sciences*, 10(11), 3671.
- TRWD. (2023). *Tarrant Regional Water District Integrated Water Supply Plan*. Fort Worth, Texas <https://www.trwd.com/resource/eagle-mountain-lake/>
- TWDB. (2022a). <https://www.twdb.texas.gov/waterplanning/swp/2022/index.asp>
- TWDB. (2022b). TWDB (2022). "2012 State Water Plan". Texas Water Development Board. Available online at: <http://www.twdb.texas.gov/waterplanning/swp/2022/docs/SWP22-Water-For-Texas.pdf> (Accessed February 13, 2022).
- UN. (2021). *United Nations* <https://sdqs.un.org/sites/default/files/2021-05/UN-SG-Action-Plan-Water-Action-Decade-web-0.pdf>.
- United States Census Bureau. (2022). <https://www.census.gov/newsroom/press-releases/2022/2022-population-estimates.html#:~:text=Changes%20are%20in%20bold,.components%20of%20change%20released%20today>.

- USDA. (2020). <https://www.nrcs.usda.gov/resources/data-and-reports/gridded-soil-survey-geographic-gssurgo-database>
- USEPA. (2022). *United States Environmental Protection Agency-* <https://www.epa.gov/watersense/statistics-and-facts>
- Vagheei, H., Laini, A., Vezza, P., Palau-Salvador, G., & Boano, F. (2022). Ecohydrologic modeling using nitrate, ammonium, phosphorus, and macroinvertebrates as aquatic ecosystem health indicators of Albaida Valley (Spain). *Journal of Hydrology: Regional Studies*, 42, 101155.
- Van Den Besselaar, E. J., Tank, A. M. K., Van Der Schrier, G., Abass, M. S., Baddour, O., Van Engelen, A. F., Freire, A., Hechler, P., Laksono, B. I., & Jilderda, R. (2015). International climate assessment & dataset: Climate services across borders. *Bulletin of the American Meteorological Society*, 96(1), 16-21.
- van Dijk, S., Lounsbury, A. W., Hoekstra, A. Y., & Wang, R. (2020). Strategic design and finance of rainwater harvesting to cost-effectively meet large-scale urban water infrastructure needs. *Water research*, 184, 116063.
- Wang, L., Zhang, J., Shu, Z., Wang, Y., Bao, Z., Liu, C., Zhou, X., & Wang, G. (2021). Evaluation of the ability of CMIP6 global climate models to simulate precipitation in the Yellow River Basin, China. *Frontiers in Earth Science*, 9, 751974.
- WMO. (2022). Provisional State of the Global Climate in 2022.
- Woltemade, C. J., Hawkins, T. W., Jantz, C., & Drzyzga, S. (2020). Impact of changing climate and land cover on flood magnitudes in the Delaware River Basin, USA. *JAWRA Journal of the American Water Resources Association*, 56(3), 507-527.
- Xian, C., Gong, C., Lu, F., Wu, H., & Ouyang, Z. (2022). The evaluation of greenhouse gas emissions from sewage treatment with urbanization: Understanding the opportunities and challenges for climate change mitigation in China's low-carbon pilot city, Shenzhen. *Science of The Total Environment*, 158629.
- Yang, D., Yang, A., Qiu, H., Zhou, Y., Herrero, H., Fu, C.-S., Yu, Q., & Tang, J. (2019). A citizen-contributed GIS approach for evaluating the impacts of land use on hurricane-Harvey-induced flooding in Houston area. *Land*, 8(2), 25.
- Yang, S., Tan, M. L., Song, Q., He, J., Yao, N., Li, X., & Yang, X. (2023). Coupling SWAT and Bi-LSTM for improving daily-scale hydro-climatic simulation and climate change impact assessment in a tropical river basin. *Journal of Environmental Management*, 330, 117244.
- Yaoming, L., Qiang, Z., & Deliang, C. (2004). Stochastic modeling of daily precipitation in China. *Journal of Geographical Sciences*, 14, 417-426.
- Yu, J., Noh, J., & Cho, Y. (2020). SWAT model calibration/validation using SWAT-CUP I: Analysis for uncertainties of objective functions. *Journal of Korea Water Resources Association*, 53(1), 45-56.
- Yuan, L., & Forshay, K. J. (2022). Evaluating Monthly Flow Prediction Based on SWAT and Support Vector Regression Coupled with Discrete Wavelet Transform. *Water*, 14(17), 2649.
- Zhang, D., Sial, M. S., Ahmad, N., Filipe, A. J., Thu, P. A., Zia-Ud-Din, M., & Caleiro, A. B. (2020). Water scarcity and sustainability in an emerging economy: a management perspective for future. *Sustainability*, 13(1), 144.

- Zhang, Y., Qi, J., Pan, D., Marek, G. W., Zhang, X., Feng, P., Liu, H., Li, B., Ding, B., & Brauer, D. K. (2022). Development and testing of a dynamic CO<sub>2</sub> input method in SWAT for simulating long-term climate change impacts across various climatic locations. *Journal of Hydrology*, *614*, 128544.
- Zhao, H., Li, H., Xuan, Y., Li, C., & Ni, H. (2022). Improvement of the SWAT Model for Snowmelt Runoff Simulation in Seasonal Snowmelt Area Using Remote Sensing Data. *Remote Sensing*, *14*(22), 5823.
- Zscheischler, J., Martius, O., Westra, S., Bevacqua, E., Raymond, C., Horton, R. M., van den Hurk, B., AghaKouchak, A., Jézéquel, A., & Mahecha, M. D. (2020). A typology of compound weather and climate events. *Nature reviews earth & environment*, *1*(7), 333-347.



# VITA

## Personal Background

Daniel Ayomikun Ayejoto

Fort Worth, Texas

## Education

2017 Bachelor of Science, Industrial Chemistry, University of Ilorin  
2023 Master of Science, Environmental Science, Texas Christian University

## Experience

2022-2024 Teaching Assistant, Texas Christian University  
2021 Research Assistant, University of Chinese Academy of Sciences  
2019 Research Assistant, Chukwuemeka Odumegwu Ojukwu University, Nigeria  
2019 Research Intern, University of Ilorin, Nigeria

## Publications

Ayejoto, D. A., Agbasi, J. C., Egbueri, J. C., & Echefu, K. I. (2022). Assessment of oral and dermal health risk exposures associated with contaminated water resources: an update in Ojoto area, southeast Nigeria. *International Journal of Environmental Analytical Chemistry*, 1-21.

Ayejoto, D. A., Agbasi, J. C., Egbueri, J. C., & Abba, S. I. (2023). Evaluation of oral and dermal health risk exposures of contaminants in groundwater resources for nine age groups in two densely populated districts, Nigeria. *Heliyon*, 9(4).

Ayejoto, D. A., Agbasi, J. C., Nwazelibe, V. E., Egbueri, J. C., & Alao, J. O. (2023). Understanding the connections between climate change, air pollution, and human health in Africa: Insights from a literature review. *Journal of Environmental Science and Health, Part C*, 41(3-4), 77-120.

## Awards

2023 \$3,000 - ENSC graduate research grant award, Department of Environmental Sciences, Texas Christian University

2023 \$400 - Graduate Student Travel Grant, College of Science and Engineering, Texas Christian University

2022 \$3,000- Open Access Fund, Texas Christian University Library

## **ABSTRACT**

### **Modeling the impact of climate change on the hydrology of Eagle Mountain Lake, Texas.**

By Daniel Ayomikun Ayejoto, M.S., 2024  
College of Science and Engineering  
Texas Christian University

Thesis Advisors: Dr. Gehendra Kharel, Assistant Professor of Environmental Science

Dr. Brendan Lavy, Assistant Professor of Environmental

Science Committee Member: Prof. Birmingham Michele, Assistant Professor of Environmental Science

This study investigates the modeling of climate change impacts on streamflow dynamics within the Upper West Fork Trinity Watershed, employing the Soil and Water Assessment Tool (SWAT). The study begins with the successful development and validation of a SWAT model for the historical period (1990-2022), demonstrating strong agreement between simulated and observed streamflow data. Subsequently, the model is utilized to assess the impacts of projected climate change scenarios (2030s and 2080s) under different Shared Socioeconomic Pathways (SSPs) on streamflow dynamics.

The findings reveal consistent trends of increasing average temperatures across all scenarios, with temperature projections aligning with global warming patterns observed in various watersheds worldwide. Moreover, projected precipitation patterns indicate both increases and decreases, leading to increased uncertainty and variability in future climatic conditions. These changes in temperature and precipitation translate into significant

alterations in streamflow dynamics within the watershed. Despite anticipated increases in average annual precipitation, the model projects a decrease in streamflow, particularly during spring and early summer months, which could impact water availability in the Eagle Mountain Lake reservoir. Specifically, the average annual streamflow in the watershed is projected to decrease by 17% to 20% under future climatic conditions compared to the 2003 – 2022 observed streamflow. However, projections also suggest an increase in streamflow during summer, fall, and winter months by 18%, 12%, and 3.6% respectively, potentially offsetting spring deficiencies in the reservoir but also raising concerns about riverine and lake flooding.

Overall, this study provides valuable insights into the potential impacts of climate change on water resources within the Upper West Fork Trinity Watershed, highlighting the importance of adaptive management strategies in mitigating the effects of evolving environmental conditions.